JOURNAL OF PETROLOGY | VOLUME 51 | NUMBER 6 | PAGES 1267–1295 | 2010 | doi:10.1093/petrology/egq019

Melting Relations of MORB–Sediment Mélanges in Underplated Mantle Wedge Plumes; Implications for the Origin of Cordilleran-type Batholiths

ANTONIO CASTRO[1]*, TARAS GERYA[2,3], ANTONIO GARCÍA-CASCO[4], CARLOS FERNÁNDEZ[5], JUAN DÍAZ-ALVARADO[5], IGNACIO MORENO-VENTAS[1] AND IRENA LÖW[2]

[1]DEPARTAMENTO DE GEOLOGÍA, UNIVERSIDAD DE HUELVA, HUELVA, SPAIN

[2]GEOPHYSICAL FLUID DYNAMICS GROUP, INSTITUTE OF GEOPHYSICS, DEPARTMENT OF EARTH SCIENCES, SWISS FEDERAL INSTITUTE OF TECHNOLOGY (ETH-ZURICH), 8093 ZURICH, SWITZERLAND

[3]GEOLOGY DEPARTMENT, MOSCOW STATE UNIVERSITY, 119899 MOSCOW, RUSSIA

[4]DEPARTAMENTO DE MINERALOGÍA Y PETROLOGÍA AND INSTITUTO ANDALUZ DE CIENCIAS DE LA TIERRA (CSIC-UGR), UNIVERSIDAD DE GRANADA, GRANADA, SPAIN

[5]DEPARTAMENTO DE GEODINÁMICA Y PALEONTOLOGÍA, UNIVERSIDAD DE HUELVA, HUELVA, SPAIN

RECEIVED APRIL 26, 2009; ACCEPTED APRIL 5, 2010
ADVANCE ACCESS PUBLICATION MAY 7, 2010

This paper gives the results of a set of laboratory experiments designed to analyse the petrological implications of mantle wedge plumes—large buoyant structures predicted by thermomechanical numerical modelling of subduction zones. A particular design of layered capsule was used to simulate the complex multilayer formed by intense flow within the mantle wedge as predicted by numerical models. A basaltic [mid-ocean ridge basalt (MORB)-derived amphibolite] component was sandwiched between two adjacent layers of a sedimentary (Bt-rich metagreywacke) component. Conditions were fixed at temperatures of 1000–1200°C at pressures of 1·5–2·0 GPa. Our results suggest that significant volumes of hybrid, Cordilleran-type granodioritic magmas can be generated by sub-lithospheric partial melting of a mechanically mixed source. Partial melting of the end-members is not buffered, forming granitic (melting of metasediment) and trondhjemitic (melting of MORB) melts in high-variance assemblages Melt + Grt + Pl and Melt + Grt + Cpx, respectively. However, the composition of melts formed from partial melting of metasediment–MORB mélanges is buffered for sediment-to-MORB ratios ranging from 3:1 to 1:3, producing liquids of granodiorite to tonalite composition along a cotectic with the lower-variance phase assemblage Melt + Grt + Cpx + Pl. Our model explains the geochemical and isotopic characteristics of Cordilleran batholiths. In particular, it accounts for the observed decoupling between major element and isotopic compositions. Large variations in isotopic ratios can be inherited from a compositionally heterogeneous source; however, major element compositions are more strongly dependent on the temperature of melting rather than on the composition of the source.

KEY WORDS: *granodiorite; tonalite; cordilleran batholiths; melting experiments; subduction; silicic plumes; mélange*

INTRODUCTION

The production of large silicic batholiths, dominantly composed of rocks of granodiorite to tonalite composition, is the most outstanding consequence of plate subduction

*Corresponding author. E-mail: dorado@uhu.es

below active continental margins (Wyllie, 1977). These rock assemblages are normally referred to as Cordilleran-type granitoids; they are magnesian, calc-alkalic to calcic granitoids according to the Frost *et al.* (2001) classification scheme. For simplicity they are referred to as Cordilleran-type granitoids subsequently. In addition to important additions from underplated mafic magmas in intracratonic areas (Frost *et al.*, 2001), there is a general consensus about the contribution of Cordilleran-type batholiths to the growth of the continents since Late Archaean times (Condie, 1997; Hawkesworth & Kemp, 2006). Consequently, deciphering the petrogenesis of Cordilleran-type batholiths is crucial to our understanding of the generation and evolution of the continents.

Any petrogenetic model for Cordilleran-type magmatism at continental active margins must satisfy the important observation that both intrusive and extrusive rocks have hybrid mantle–crust geochemical signatures, as evidenced by their Sr and Nd isotopic compositions (Fig. 1). Available Nd–Sr isotope data support the involvement of recycled crustal components (i.e. sediments) and unaltered mantle materials (Allègre & Ben Othman, 1980; De Paolo, 1981; McCulloch & Gamble, 1991). Geochemical characteristics of Cordilleran-type magmatic rocks, such as their high Ce/Yb and Sr/Y ratios, suggest that the magmas equilibrated with garnet in a hybrid-source region, requiring relatively high pressure of melt formation. Thus the application of any thermal model for Cordilleran-type batholith generation requires the existence of a recycled sedimentary reservoir in a deep source region, at either deep crustal or mantle conditions (>1 GPa). Furthermore, petrogenetic models must be able to produce the large isotopic (e.g. Sr and Nd) heterogeneities displayed by the granitoids while keeping their major element composition nearly constant (i.e. granodiorite–tonalite; e.g. Pankhurst *et al.*, 1999). The solution of this paradox is critical to understanding the origin of batholiths.

There are numerous genetic models for Cordilleran-type batholiths. They can be classified in two broad categories, intra-crustal models and extra-crustal models, depending on the location of the source region and the provenance of the continental crustal component. Both models satisfy one important observational feature of Cordilleran-type batholiths: they constitute distinctive features of active continental margins whereas they are rare in intra-oceanic arcs. These crustal components may be supplied directly by the melting and/or assimilation of the continental crust (intra-crustal models) or by subducted sediments derived from continental crustal denudation (extra-crustal models). In both cases silicic melts may evolve within crustal reservoirs by means of further melting, assimilation, storage, and homogenization (MASH) processes (Hildreth & Moorbath, 1988).

Intra-crustal models postulate that whatever the process involved in the generation of Cordilleran batholiths, they are produced within the continental crust. Currently accepted intra-crustal models include: (1) assimilation of continental crustal rocks by basalt magmas (e.g. De Paolo, 1981; Patiño-Douce, 1995); (2) coupled magma mixing and crustal assimilation, involving hydrous basalts and continental crustal melts (Thompson *et al.*, 2002); (3) continental crustal melting fluxed by fluids released from crystallizing wet basalts (Annen *et al.*, 2006).

Assimilation of pelitic sediments by basaltic magmas can yield liquid compositions approaching those of intermediate granitoid rocks, as demonstrated in previous experimental studies (Patiño-Douce, 1995; Castro *et al.*, 1999; Patiño-Douce, 1999). Experimental studies and thermal modelling indicates that a basalt-to-crust ratio of about 1:1 is required to satisfy thermal and compositional constraints (Patiño-Douce, 1995; Annen *et al.*, 2006). However, the geological record provides little support for this process. Gabbro–diorite rocks (from zoned calc-alkalic plutons), which occur commonly at pluton margins in direct contact with metasediments, do not show significant geochemical or mineralogical indications of assimilation. For example, Castro *et al.* (2003) showed that interaction between a wet basalt (appinite) and upper crustal migmatites produced only minor amounts of granitoid melt, which has a monzonitic–monzodioritic rather than a granodioritic–tonalitic composition. However, assimilation can locally be an efficient process when granodiorites and tonalites are in contact with metasediments at the level of emplacement (Ugidos & Recio, 1993; Fowler *et al.*, 2001). The efficiency of this process is enhanced by coupled dehydration reactions and xenolith disaggregation (Beard *et al.*, 2005).

Two additional intra-crustal models involve the addition of water to the hybrid-source system. This process is fundamental to reduce the solidus temperature and to enhance the fertility of the source, but it inexorably leads to the formation of water-rich magmas. Water-rich silicic magmas of broadly dacitic to rhyolitic composition (Moore & Carmichael, 1998; Costa *et al.*, 2004; Grove *et al.*, 2005) and some peculiar intrusions of tonalitic–granodioritic composition (e.g. Adamello Massif; Blundy & Sparks, 1992) can be generated by this mechanism in active continental margins. However, the general case for the Cordilleran-type batholiths is one of strong water-undersaturation (Presnall & Bateman, 1973) even for near-solidus residual liquids formed after magma crystallization. A universal feature of these Cordilleran-type batholiths is the presence of late-stage, interstitial hydrous minerals (hornblende and/or biotite), and euhedral to subhedral, zoned plagioclase feldspar. Amphibole polycrystalline clots, derived from pyroxene reaction (Castro & Stephens, 1992), are also common. These textural relations

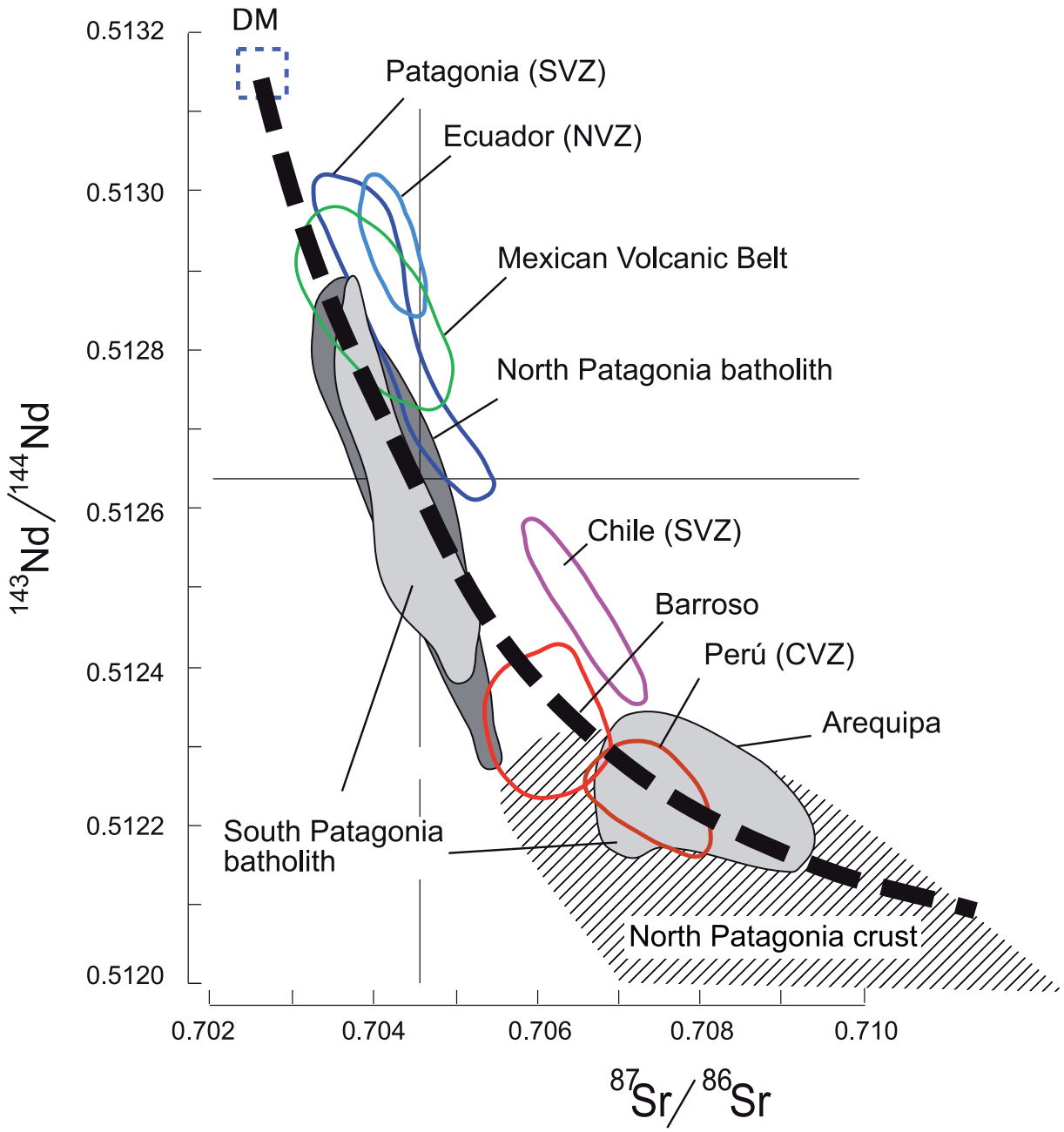

Fig. 1. Initial Sr–Nd isotope ratios of Jurassic–Tertiary batholiths and volcanic rocks from the Andes. The field for North Patagonian crust is from Pankhurst *et al.* (1999) at 135 Ma. Data for the South Patagonia batholith are from Hervé *et al.* (2007) and from the North Patagonia batholith from Pankhurst *et al.* (1999). Bold dashed line is a hypothetical mixing trend between an end-member DM component (MORB) and a crustal component. DM, depleted mantle; NVZ, Northern Volcanic Zone, Andes; CVZ, Central Volcanic Zone, Andes; SVZ, Southern Volcanic Zone, Andes.

are the consequence of very low water contents. The comparison between experimental phase equilibria (Maaloe & Wyllie, 1975; Naney, 1983; Scaillet & Pichavant, 2003) and natural crystallization sequences strongly suggests that the initial water contents of Cordilleran-type magmas are less than 2 wt % H_2O. The temperature required to stabilize these water-poor melts (>1000°C) exceeds the maximum temperature predicted by basalt-fluxed models in the sub-arc lower continental crust. A first-order estimate indicates that the water supplied (*c.* 1 wt %) by hydrous minerals (i.e. amphibole and biotite) to the hybrid source is enough to satisfy the low

water content (*c.* 2 wt %) of tonalite and granodiorite magmas produced by 50% melting. However, according to heat transfer models (Petford & Gallagher, 2001; Annen & Sparks, 2002), the heat provided by the intrusion of wet basalt at temperatures of 1100–1240°C (Pichavant *et al.*, 2002) in the lower crust is not sufficient to produce high melt fractions from an amphibole-bearing protolith. Detailed numerical models that simulate the sequential arrival of wet basaltic sills at varied emplacement rates and depths (Annen *et al.*, 2006) indicate that basalt-to-crust ratios of about 3:2 in the lower crust are needed to increase local temperatures to 1100°C and to produce high melt fractions (>0·5 for typical intrusion rates of 5 mm/year) corresponding to water-rich andesitic and dacitic compositions.

The second group of models (extra-crustal models) propose formation of silicic magmas in the lithospheric mantle either by differentiation of basaltic–andesitic parental magmas, generated by mantle melting, or by melting of silicic materials that were subducted and recently emplaced into the supra-subduction zone mantle wedge by diapiric structures rooted in the subduction channel (Gerya & Stoeckhert, 2006; Gorczyk *et al.*, 2007*a*). Annen *et al.* (2006) discussed the role of differentiation of mantle-derived wet basalt or basaltic andesite magmas in producing silicic magmas within the continental crust. They concluded that this process, coupled with interaction with crustal rocks and melts, could produce the water-rich silicic magmas that characterize many volcanic arcs. However, Cordilleran-type plutonic rocks are characterized by strong water-undersaturation, with the implication that the temperatures of magma generation may exceed those of intra-crustal models.

We have suggested in a previous study (Castro & Gerya, 2008) that melting of subducted mélanges is a process capable of generating Cordilleran-type batholiths. This hypothesis is further explored in this study by means of new experimental data and numerical experiments.

In applying intra-crustal or extra-crustal (mantle) models for the generation of Cordilleran-type magmas, the significance of the time–composition variations of Cordilleran-type batholiths must be taken into account. Repeated episodes of batholith generation at continental margins should record distinctive patterns of time–composition evolution depending on the location of the source region in either the continental crust or the mantle wedge. Although a subducted crustal component can be injected sporadically into the mantle wedge, allowing this hybrid-source region to remain fertile for intermediate magma production for protracted time periods, the continental crustal source should become progressively more refractory by successive extraction of melt, reducing its fertility with time. To show the importance of this time-dependent aspect in deciphering active continental margin magmatism, we summarize below the characteristic features of Cordilleran batholiths from the active margins of the Americas.

Most batholiths exhibit a narrow compositional range from granodiorite to tonalite within the most voluminous bodies (>90 vol. %). These rocks have limited major element compositional ranges (SiO_2 63–70 wt %, FeO 2–5 wt %, MgO 1–3 wt %, CaO 3–5 wt %, Na_2O 2–4 wt % and K_2O 2–4 wt %). Large batholiths of more 1000 km in length are composed of multiple intrusions that are elongated parallel to the trench. Although the peak of magmatic activity occurred during the Cretaceous, the ages of the batholiths span long periods of time of about 40 and 31 Myr in the Sierra Nevada and Peninsular Ranges batholiths respectively (Lee *et al.*, 2007), 200 Myr in the Chilean Coastal batholith (Parada *et al.*, 1999), 130 Myr in the North Patagonian batholith (Pankhurst *et al.*, 1999) and 150 Myr in the South Patagonian batholith (Hervé *et al.*, 2007). During these long time intervals the major element compositions of the intrusions remain unchanged. However, there is a marked compositional evolution with time of Sr and Nd isotopic ratios, denoting an increase in the mantle contribution with time. For instance, drastic changes from $\varepsilon_{Nd} = -4$ to $+6$ are characteristic of plutons forming the South American batholiths (Pankhurst *et al.*, 1999, and references herein), evolving to positive values from Carboniferous to Tertiary time. This time–composition evolution seems incompatible with the assimilation of sub-arc continental crustal rocks as the cause of the silicic magmatism. It also conflicts with their derivation from a volumetrically limited source within the continental crust. In the case of assimilation, a parallel evolution to compositions richer in silica and alkalis on the one hand, and with more radiogenic Sr and less radiogenic Nd on the other, is expected. For the case of an intra-crustal origin (basalt-fluxed models), a localized source within the continental crust will evolve to more refractory compositions as a result of the continuous extraction of melts over tens of million years. These features have been attributed to lithospheric imprints transferred to the magmas by the effects of subduction (Pankhurst *et al.*, 1999). The uniform major element composition of magmas emplaced in narrow zones less than 100 km wide over more than 100 Myr (e.g. Patagonia) strongly suggests a constant or episodic supply of new, fresh basaltic magma to the source region, as expected in the active subduction zones of the western continental margins of the Americas during the last 200 Ma.

This study is an experimental and thermomechanical test of an extra-crustal model for the generation of Cordilleran-type magmas. Our test expands the thermal conditions of crustal models to lithospheric mantle temperatures, affecting water-poor protoliths composed of mixed subducted metabasite and metasediment. A mixed

protolith of this type, satisfying composition, water content and hybrid isotopic fingerprints, is found in subduction mélanges (Shreve & Cloos, 1986) formed at the subduction channel by accretion of hydrated oceanic crust and sediments. Similar mixed subducted protoliths are expected in the case of subduction erosion of continental fore-arc basement and/or cover (von Huene & Scholl, 1991), which have been identified as the potential source for the recycled components of Cordilleran-type rocks (Stern, 1991). Themomechanical modelling of subduction zones (Gerya & Yuen, 2003*b*; Gerya *et al.*, 2004; Currie *et al.*, 2007) predicts that these subducted fertile materials can be transported as buoyant diapiric structures from the subduction channel to the hot region of the sub-arc mantle wedge, where high melt fractions can be attained. It will be shown that our results account for the relevant geochemical and thermal requirements emerging from recent studies on Cordilleran-type batholiths, and that the proposed alternative model is compatible with classical models that consider differentiation of mantle-derived magmas and melting–assimilation of continental crustal rocks.

MANTLE WEDGE PLUMES AS THE SOURCE OF CORDILLERAN-TYPE BATHOLITHS

The subduction channel, which is composed dominantly of oceanic crust and sediments (Shreve & Cloos, 1986), is a composite source that potentially could produce silicic magmas on melting. However, this hypothesis has received little attention because of the absence of sufficiently detailed models simulating the coupled thermal, rheological and petrological evolution of subduction systems. New petrological–thermomechanical subduction models have predicted a complex structure in the mantle wedge with the formation of large ascending diapirs ('cold plumes'; Gerya & Yuen, 2003*a*; Gerya *et al.*, 2004) as a result of Raleigh–Taylor instabilities caused by hydration and melting atop the subducting slab. The stability and compositional variations of such thermal–chemical plumes above slabs were investigated numerically for a variety of tectonic settings, including ocean–ocean (Gerya & Yuen, 2003*a*; Gerya *et al.*, 2004, 2006; Gorczyk *et al.*, 2007*a*, 1007*b*; Nikolaeva *et al.*, 2008), ocean–continent (Gerya & Stoeckhert, 2006; Currie *et al.*, 2007; Gorczyk *et al.*, 2007*c*; Gerya *et al.*, 2008), and continent–continent (Gerya *et al.*, 2008) collision with both retreating and advancing subduction. It has been demonstrated (e.g. Gerya & Yuen, 2003*a*; Gerya *et al.*, 2006; Currie *et al.*, 2007) that such plume structures could be common in subduction zones, caused by the positive buoyancy of hydrated, partially molten mantle and crustal rocks subducted atop slabs. The geophysical implications of mantle wedge plumes were evaluated by Gerya *et al.* (2006), who suggested that thermal–chemical plume structures may explain the significant localized positive and negative seismic velocity anomalies present in mantle wedges.

The numerical experiments of Gerya *et al.* (2006) show that two distinct types of plume can be generated in the mantle wedge, as follows.

(1) Unmixed plumes form a few kilometres above the slab; these consist of hydrated, partially molten mantle located at a distance from the slab, which is therefore not mechanically mixed with subducted crustal rocks. Such plumes are expected to carry a pronounced slab fluid signature and commonly provide major contribution for magmatic activity in ocean–ocean (Nikolaeva *et al.*, 2008) and ocean–continent (Gorczyk *et al.*, 2007*c*; Gerya *et al.*, 2009) subduction zones.

(2) Mixed plumes form directly atop the slab and consist of hydrated partially molten mantle and recycled oceanic crust and sediments. Such plumes are expected to carry a strong crustal signature and can be episodically present in all types of subduction zone (e.g. Gerya & Yuen, 2003*a*; Gerya & Stoeckhert, 2006; Currie *et al.*, 2007; Gorczyk *et al.*, 2007*a*; Gerya *et al.*, 2008, 2009).

All types of mantle wedge plume will actively produce melts during their growth, associated with both decompression and heating of plume material supplied from the slab in either a continuous or an episodic manner (Gerya & Yuen, 2003*a*; Gerya *et al.*, 2004; Gerya & Stoeckhert, 2006; Gorczyk *et al.*, 2007*a*, 2007*c*).

Mixed thermal–chemical plumes can in particular transport rock mélanges that originated in the subduction channel (Shreve & Cloos, 1986) to hot regions within the mantle wedge. Consequently, they offer a new model for the generation of arc magmas that must be confirmed by laboratory experiments. A preliminary study on melting of composite mélanges (Castro & Gerya, 2008) showed partial experimental results with a single mélange composition (50% sediment) and further reaction of the resultant silicic melts with mantle peridotite. The main implication of these experiments is that partially molten mantle wedge plumes may survive reaction with the surrounding peridotite mantle. The reaction aureole is composed of hybridized ultramafic mantle material, devoid of olivine, that may serve as a potential source for the hydrous mafic magmas that occur in minor amounts in most arcs. Interestingly, the silicic melt of the interior of the plume remains unchanged by reaction with the surrounding mantle. These experiments tell us about the chemical stability of the silicic plume. However, to analyze the effect of changing pressure and temperature on magma compositions requires enlarging the experimental dataset to new

conditions. Another point of interest, not checked by Castro & Gerya (2008), is the effect of the fraction of sediments in the mélange on the composition of the resultant melts. In this study we report the results of a comprehensive study of experimentally determined phase equilibria, over a wide range of pressures (1·5–2·0 GPa) and temperatures (1000–1200°C), using varied proportions of the sedimentary component in the mixed source.

Numerical experiments with subducted mélanges in active continental margins: stationary and underplated plumes

To simulate the evolution of a subducting slab beneath a continental plate, including the effects of sediment and felsic crust subduction, a number of numerical experiments were conducted by Sizova *et al.* (2009). Their models consider a 2D, vertical profile through a hypothetical subduction orogen, parallel to the convergence vector. The size of the modelled area was 200 km in depth and 4000 km in length, and the convergence rate 5 cm/a. The modelled oceanic crust included an upper layer of spilitized basalts (2 km) overlying a layer of gabbros (5 km), and the initial thickness of the continental crust was 30 km. A sedimentary wedge was placed at the transition between the continental and oceanic lithosphere. A non-uniform rectangular grid was employed, with a high-resolution area (2 km × 2 km) in the centre of the section, whereas in the rest of the area the resolution was 10 km × 2 km. The models considered free slip at the top and side boundaries, external free slip at the lower boundary (i.e. free slip is guaranteed for a boundary located 1000 km below the lower boundary of the model), erosion and sedimentation processes at the surface of the crust, dehydration–hydration processes, melting of rocks, fluid and melt migration processes, and a viscoplastic rheology for the distinct layers. They included the 2D continuity equation for creeping flow with time-dependent density. Thermal and chemical buoyancy forces and mechanical heating were considered using the heat conservation equation. The numerical experiments were conducted using the I2VIS numerical code of conservative finite differences with a non-diffusive marker-in-cell technique to model multiphase flow (Gerya & Yuen, 2003*a*). Further details of the experimental set-up and procedure have been given by Gorczyk *et al.* (2007*c*) and Sizova *et al.* (2009).

Figure 2 shows one of the characteristic subduction regimes obtained in the Sizova *et al.* (2009) experiments, which is associated with the development of a large sedimentary plume (e.g. Currie *et al.*, 2007). This regime is characterized by advancing subduction, shortening and thickening of the overriding plate and steep slab inclination. As demonstrated by van Huenen *et al.* (2000), slab inclination strongly depends on the relative plate motion and slab flattening is promoted by an active overthrusting of the overriding continental plate. In contrast, in the Sizova *et al.* (2009) model the overriding plate position remains fixed, which often results in relatively steep slab angles. The distinct feature of the Sizova *et al.* (2009) model is the growth of a volcanic rock sequence on the top of the overriding plate (Fig. 2) in response to melt extraction from various partially molten regions (Gorczyk *et al.*, 2007*c*; Nikolaeva *et al.*, 2008; Sizova *et al.*, 2009) within the mantle wedge: hydrated peridotite, subducted oceanic crust and sediments. All of these melt sources are present in different proportions both atop the slab and inside the growing sub-lithospheric plume.

By conducting a series of experiments Sizova *et al.* (2009) tested the geodynamic consequences of the rheological weakening effects of fluids and melts. Pore fluid pressure ($\lambda_{fluid} = 1 - P_{fluid}/P_{solid}$) is an important parameter in the tectonic evolution of the modelled subduction zone. Low values of λ_{fluid} (<0·1) (i.e. high fluid pressures) allow deformation of the subducted sediments and the growth of a large accretionary wedge (Sizova *et al.*, 2009, fig. 6). The weak subducting slab interface results in a low degree of coupling between the plates, with rapid trench retreat and intra- and back-arc extension of the upper plate. The amount of subducted sediments in the model is small and the resulting magmas show minimal participation of either sediment or basalt from the subducting slab in the melting zone. However, when λ_{fluid} is >0·1 (i.e. for low to moderate fluid pressures) the subducting slab interface is generally stronger, the plates are more rheologically coupled and larger volumes of (stiffer) sediments are subducted atop the slab (Sizova *et al.*, 2009, fig. 6). Subduction of a large volume of sediment is necessary (Currie *et al.*, 2007) for the generation of silicic plumes of partially molten sediment and basalt that underplate the continental lithosphere (Fig. 2) and are heated from the surrounding hot mantle.

A second important parameter controlling the development of mantle wedge plumes is the melt-related weakening factor ($\lambda_{melt} = 1 - P_{melt}/P_{solid}$), which affects the properties of the lithosphere above the area of melt extraction from partially molten mantle wedge regions (e.g. Nikolaeva *et al.*, 2008; Sizova *et al.*, 2009). Three types of sedimentary–basaltic plumes were obtained in the numerical experiments (see Castro *et al.*, 2009, fig. 7; Sizova *et al.*, 2009, figs 6 and 7): ascending plumes that break through the continental lithosphere, stationary plumes that remain in the localized area of mantle wedge corner, often associated with rigid body rotation phenomena ('subduction wheel', Gorczyk *et al.*, 2007*a*), and plumes that underplate the lithosphere, extending horizontally below the overriding plate (Currie *et al.*, 2007; Gorczyk *et al.*, 2007*c*; Gerya *et al.*, 2009; Sizova *et al.*, 2009, fig. 6). Ascending plumes develop under moderate to high melt-related weakening of the overlying lithosphere

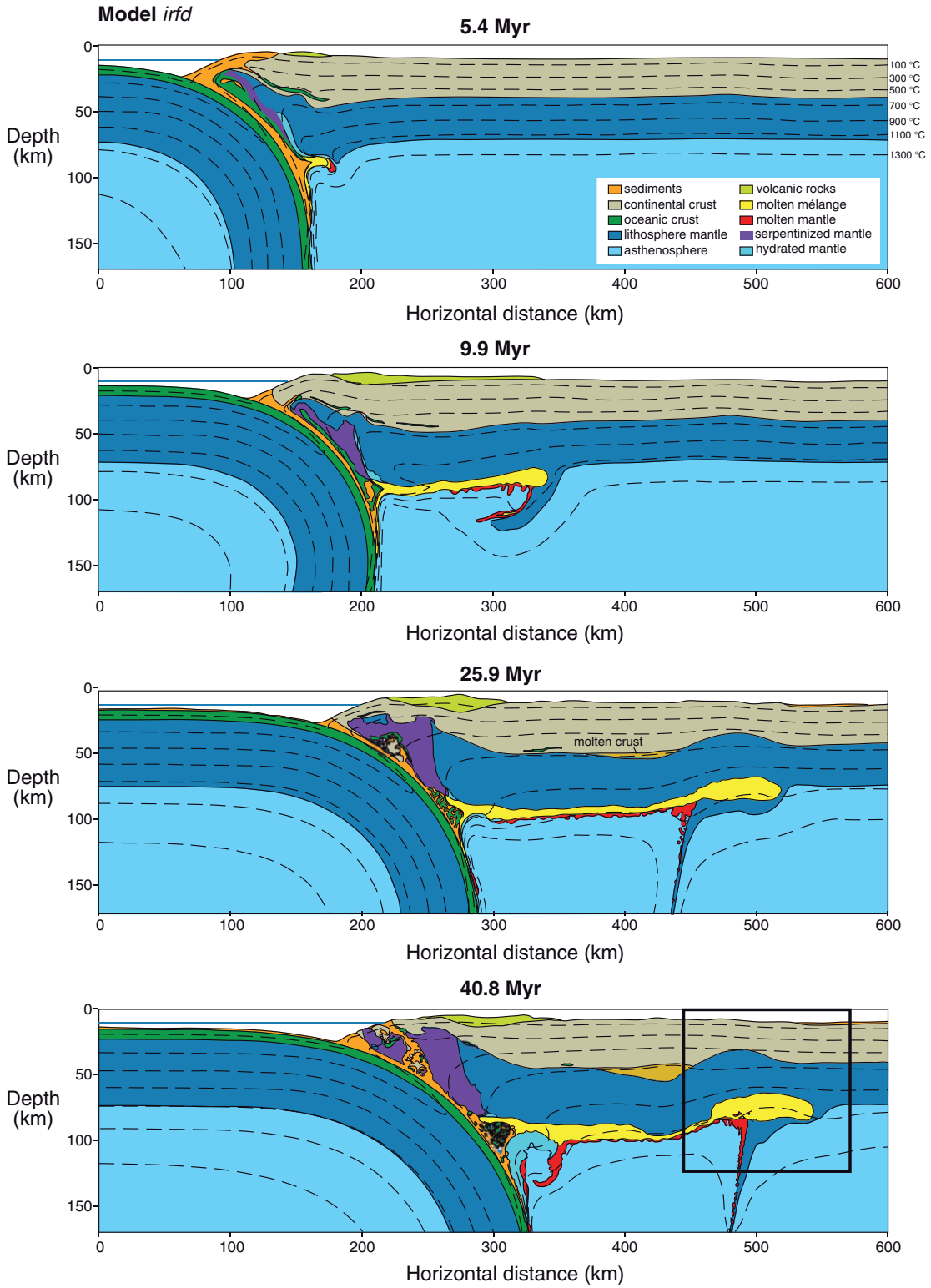

Fig. 2. Results of the numerical experiment showing the development of a cold 'plume' underplating the continental lithosphere of the overriding plate. The model considers $\lambda_{fluid} = 1$ and $\lambda_{melt} = 0{\cdot}1$ (see text for explanation). A mature plume head is generated less than 26 Myr after the start of the subduction process. The bottom figure shows the essentially underplated plume 40·8 Myr after subduction initiation; that is, around 15 Myr after a mature plume head was generated. The numerical experiment indicates that the geometry of the underplated plume can survive for as much as 25–30 Myr. Therefore, the plume head, which constitutes a large repository of subducted mélange materials, can have a long residence time within the mantle wedge, which has profound petrogenetic implications as discussed in the text. Large square in the bottom figure refers to Fig. 11. Model results from Sizova *et al.* (2009)

($\lambda_{melt} < 0{\cdot}01$), which is weakened along localized zones permitting very rapid ascent of the plume to crustal depths (Castro *et al.*, 2009, fig. 7). The temperature in the ascending plumes does not exceed 900°C. Similar results are obtained for stationary plumes ($\lambda_{melt} \geq 0{\cdot}01$ and $0{\cdot}3 > \lambda_{fluid} > 0{\cdot}1$; Sizova *et al.*, 2009, figs 6 and 7), where the subducted material is trapped in a vortex forming in relatively cold hydrated mantle wedge corner. In contrast, in models of underplating plumes ($\lambda_{melt} \geq 0{\cdot}01$ and $\lambda_{fluid} \geq 0{\cdot}3$; Sizova *et al.*, 2009, fig. 7), ascent of the plume is prevented by the strong overlying lithosphere (Currie *et al.*, 2007), which is placed under compression, pushing the plume head towards the back-arc region and forcing it to extend horizontally beneath the shortening continental lithosphere (Fig. 2). As follows from the distribution of volcanic rocks above the plume (light green material forming atop the overriding plate in Fig. 2) the most significant melt production inside the plume is located in the area where new plume material is detached from the slab and it is subjected to decompression and heating. The plume head, generated 10–25 Myr after the start of the subduction process, constitutes a huge accumulation (80–100 km in length and 20 km in thickness) of partially molten material including sediment, continental crust and basalt. An important feature of these underplating plumes is their large residence time within the mantle wedge (several million years; see below) and the high T reached at moderate pressures. Temperatures within the plume head may be higher than 1100°C in the lower third of the volume and between 900 and 1100°C in the remainder of the body at pressures of between 1·5 and 2·0 GPa. The numerical model also predicts the presence of wet molten mantle beneath the plume head (Fig. 2). These conditions for magma generation are taken as the basis for our experimental study.

EXPERIMENTAL SET-UP AND RESULTS

Charge designs, starting materials and experimental procedures

As concluded from the numerical experiments, viscous flow inside the partially molten composite plume may mechanically mix (via stretching and duplications of layers, Gorczyk *et al.*, 2007*a*) the basalt (oceanic crust) and sedimentary components. Homogenization by viscous flow is also favoured by the large distance travelled horizontally by the plume, over more than 200 km from the subduction channel (Fig. 2). This flow may take millions to tens of millions of years (Fig. 2). Such long residence times allow thermal equilibrium to be reached with the surrounding mantle (see the isotherms crosscutting the plume structure, in Fig. 2, at 40·8 Ma). Based on these model predictions and on our previous experiments (Castro & Gerya, 2008) to model the reaction between the plume interior and the peridotite mantle, we designed a set of high-temperature experiments aimed to determine the phase relations and melt compositions at equilibrium.

Mixtures of subducted oceanic crust and sediments dominate the composition of the buoyant plumes and, consequently, we used these materials for our experimental study. Natural rock compositions were preferred instead of synthetic glasses for several reasons. First, the trace element composition is preserved and trace element concentrations in the melt (glass) can be determined and compared with actual rocks. Second, the water content is fixed by the mineral assemblage and remains unchanged in all runs. The mineral assemblage in the starting materials was selected in accordance with the conditions at which the plume materials (i.e. oceanic crust and sediments) leave the subduction channel and are introduced into the mantle wedge, forming buoyant structures. Consequently, a mid-ocean ridge basalt (MORB)-derived amphibolite and a mica-rich metagreywacke (Bt-gneiss) were used in this study. The gneiss has the typical major and trace element compositions of greywackes (Fernández *et al.*, 2008). This is very close to the average composition of Phanerozoic greywackes (Taylor & McLennan, 1985) and is considered representative of subducted sediments. The phase relations of these starting materials have been well constrained in previous experimental studies (Castro *et al.*, 2000; López & Castro, 2001). Table 1 shows their major and trace element compositions together with the composition of synthetic mélanges formed by variable mixing proportions of these two components.

The aim of the experiments was to test the ability of various mélange compositions to produce hybrid melts that can be compared with natural silicic magmas. Additionally, we evaluated the role of the intensive variables, P and T, in controlling the composition of the resultant melts. The baselines for evaluating the compositional changes were the melts formed from the pure end-member starting materials at the same P and T conditions.

Three types of capsules were designed for this study: (1) capsules containing the end-members (i.e. the amphibolite and the mica-rich gneiss) separately; (2) capsules containing homogeneous mixtures in variable weight proportions of the two end-members; (3) composite capsules containing a layer of amphibolite sandwiched between two layers of mica-rich gneiss. The conditions for the melting experiments with composite and single capsules were fixed in agreement with predictions from the numerical experiments discussed above. Although mantle wedge plumes are generated at the subduction interface at depths of more than 100 km (Gerya & Yuen, 2003*b*; Gorczyk *et al.*, 2007*a*), the pressure conditions for the melting experiments were fixed at the depth of final emplacement within the

Table 1: Major and trace element compositions of end-member starting materials and composite mélanges used in the experimental study

	Bt-gneiss[1]	Amphibolite[2]	Mél 1	Mél 2	Mél 3	Andesite[3]
X_s:	1	0	0·25	0·5	0·75	
Oxides (wt %)						
SiO_2	69·10	49·14	54·13	59·12	64·11	59·1–62·2
TiO_2	0·52	1·61	1·34	1·07	0·79	0·6–1·1
Al_2O_3	315·23	16·00	15·81	15·62	15·42	16·9–17·8
FeOt	3·77	9·84	8·32	6·81	5·29	4·3–6·4
MgO	1·51	7·17	5·76	4·34	2·93	2·4–3·8
MnO	0·04	0·22	0·18	0·13	0·09	0·1–0·2
CaO	1·28	10·70	8·35	5·99	3·64	5·2–7·7
Na_2O	3·06	3·29	3·23	3·18	3·12	2·8–4·3
K_2O	3·81	0·09	1·02	1·95	2·88	0·7–2·3
P_2O_5	0·18	0·14	0·15	0·16	0·17	0·1–0·2
LOI	1·30	0·44	0·66	0·87	1·09	
Total	99·80	98·64	98·93	99·22	99·51	
Mg-no.	0·42	0·57	0·55	0·53	0·50	
ASI	1·33	0·64	0·73	0·86	1·04	
K/(K + Ca), mol	0·64	0·00	0·07	0·16	0·32	
Trace elements (ppm)						
Sc	9·6	32·7	27·0	21·2	15·4	
V	64·5	214·6	177·1	139·5	102·0	
Cr	63·8	271·9	219·9	167·8	115·8	
Co	40·0	36·5	37·4	38·3	39·2	
Ni	16·6	80·6	64·6	48·6	32·6	
Rb	167·2	20·5	57·2	93·9	130·5	
Sr	131·8	208·4	189·3	170·1	151·0	
Y	33·1	23·6	26·0	28·3	30·7	
Zr	173·0	90·6	111·2	131·8	152·4	
Nb	10·2	19·3	17·0	14·7	12·5	
Ba	696·1	64·5	222·4	380·3	538·2	
La	32·1	6·0	12·5	19·0	25·6	
Ce	68·4	15·7	28·8	42·0	55·2	
Pr	8·3	2·3	3·8	5·3	6·8	
Nd	31·1	9·6	14·9	20·3	25·7	
Sm	7·1	3·1	4·1	5·1	6·1	
Eu	1·1	1·1	1·1	1·1	1·1	
Gd	6·4	3·8	4·4	5·1	5·8	
Tb	1·1	0·6	0·8	0·9	1·0	
Dy	5·7	4·5	4·8	5·1	5·4	
Ho	1·2	0·9	1·0	1·0	1·1	
Er	3·0	2·7	2·7	2·8	2·9	
Tm	0·4	0·4	0·4	0·4	0·4	
Yb	2·5	2·4	2·4	2·4	2·5	
Lu	0·3	0·4	0·4	0·3	0·3	

[1]Hiendelaencina Ordovician gneiss from Iberia (Castro *et al.*, 2000).
[2]MORB-derived amphibolite from the Aracena metamorphic belt (López & Castro, 2001).
[3]Range of andesites 12–17 of Green (1982, table 1).
X_s, fraction of gneisses (sedimentary component) in the mélanges. ASI, aluminium saturation index (ASI = mol $Al_2O_3/Na_2O + K_2O + CaO$).

shallow mantle, where the underplated plumes reside for long times (Fig. 2). Thus, the experiments were conducted at 1000, 1050, 1100 and 1200°C at pressures of 1·5 and 2·0 GPa. These conditions were applied for time durations of more than 10 days for the layered capsules to achieve homogeneous hybrid melts. For single capsule runs and homogeneous mixtures, durations of about 5 days were sufficient to achieve chemical equilibrium.

The experiments were conducted in a Boyd–England type piston-cylinder apparatus at the University of Huelva (Spain). A 12·5 mm (half-inch) diameter cell was used in all the experiments. Details of the design of the cell have been given by Castro *et al.* (1999). Gold capsules were used for experiments at 1000°C, and $Au_{75}Pd_{25}$ alloy capsules for experiments at 1100–1200°C. In all cases, the capsules were filled, sealed by pressure folding and introduced into MgO pressure containers. Temperatures were measured and controlled with Pt_{100}–$Pt_{87}Rh_{13}$ thermocouples wired to Eurotherm 808 controllers. Oil pressures were measured with electronic Druck PTX 1400 pressure transmitters, connected to Omron E5CK controllers. Pressure was corrected manually and maintained within a narrow range of ±5 bar oil pressure, equivalent to ±250 bar on the sample. Heating proceeded at the maximum rate allowed by the system of 100 K/min. After the desired run time, the experiments were quenched by switching the power off, assisted by an efficient water-cooling system, at a rate of more than 100 K/s. Fast cooling was essential to avoid the formation of quench phases. After quenching, the capsules were examined for tears and checked for the proximity of the thermocouple during the run. They were mounted in epoxy, cut and polished for examination by electron microprobe.

Experimental oxygen fugacity conditions were maintained close to those of the starting materials in the $Au_{75}Pd_{25}$ capsules (Hall *et al.*, 2004). Water contents in all runs were those supplied by the hydrous minerals in the starting materials. Thus, the experimental melts were water-undersaturated. A direct proportionality between the initial water content in each charge and the shortfall from 100% of microprobe analyses of the experimental glasses was observed, suggesting that water loss through the wall capsule was minimal.

Microprobe analyses were obtained with a JEOL JXA-8200 SuperProbe at the University of Huelva. A combination of silicates and oxides were used for calibration. A defocused 20 μm diameter beam was used for glass (quenched melt) analyses to minimize Na migration within the glass. In smaller melt pools in low melt fraction experiments, a smaller beam was used to avoid contamination from surrounding phases. Runs were also checked for Fe loss in the case of the $Au_{75}Pd_{25}$ alloy capsules. The total content of Fe in the long-duration experiments was estimated by mass balance and by averaging the modal

abundances of minerals and glass determined by image analysis. Similar values were obtained in each case, indicating a maximum Fe loss to the metal capsule of ~10% relative. A slightly higher value of ~16% relative loss was directly measured in a run at 1200°C (run 12, Table 2), which was completely molten. The FeO content of this melt is 5·71 wt % after 75 h at 1200°C, the initial value being 6·81 wt % FeO.

Selected capsules in which large areas of crystal-free glass were observed were used for *in situ* trace element determinations by laser ablation inductively coupled plasma mass spectrometry (LA-ICP-MS) at the University of Granada (Spain). LA-ICP-MS analyses were performed with a 213 nm Mercantek Nd-YAG laser coupled to an Agilent 7500 ICP-MS system with a shielded plasma torch, using the NIST-610 glass as standard. The ablation was carried out in a He atmosphere. The laser beam was fixed on a 95 μm wide square section. The spot was pre-ablated for 45 s using a laser repetition rate of 10 Hz and 40% output energy. Then the spot was ablated for 60 s at 10 Hz with laser output energy of 75% [see Bea *et al.* (2005) for analytical details on standards and routine analyses].

Experimental results

Figure 3 shows representative images of textures in the composite capsule runs. Systematic changes in the coexisting assemblages are consistent with changes in the P–T conditions. Garnet appears in the runs by either increasing P from 1·5 GPa to 2·0 GPa at 1100°C (runs AC08-103 and AC08-113) or by decreasing T from 1100°C to 1050°C (run AC08-109) at 1·5 GPa (Fig. 3). Garnet breakdown in favour of Opx is accomplished by a peritectic reaction of the type Grt ↔ Opx + melt at 1·5 GPa. The run closest to the liquidus is at conditions of 1100°C and 1·5 GPa and this is devoid of Grt (Fig. 3e). Noteworthy features are the euhedral habit of slightly zoned Opx crystals formed in this run (Fig. 3f) and the high proportion of melt (>80%) compared with the other runs at lower T or higher P. The boundaries between adjacent layers are preserved at the end of the run in all of the sandwich experiments (Fig. 3). These boundaries are marked by an abrupt change in the modal proportions of crystals. However, the composition of the melt (glass) across the layers is almost constant. Figure 4 shows compositional profiles of melt (glass) across layered capsules at 1000°C and 1100°C, 1·5 GPa (runs AC08-100 and AC08-103). In both cases the melts are almost identical in composition across the layered structure, confirming chemical equilibrium between the melt and the solid phases, independently of the distribution of minerals in the capsule. Even in the low melt fraction runs at 1000°C, the apparently isolated pools of melt in the amphibolite layer are equilibrated for most major elements. Melts in this layer are several times richer in K compared with the melts produced in the isolated capsule runs, showing the efficiency of ionic diffusion in homogenizing the melt composition across the layer interface.

Compared with the melts from the runs with the isolated starting materials, the melts in the composite capsules are hybridized for all the analyzed elements. In all runs, either composite layers or homogeneous mixtures, the hybrid melts are granodioritic to tonalitic in composition, peraluminous [aluminium saturation index (ASI) >1·0] and rich in K (K_2O > 3·0 wt %). An interesting result is that there is no proportional correlation between the fraction of gneiss in the starting mixture and the composition of the resulting melt. Rather, the melts are very close in composition for a wide range of end-member proportions. This is illustrated in Fig. 5 in terms of the major element compositions of melts produced at 1100°C and 2·0 GPa versus the fraction of Bt-gneiss (X_s = mass of gneiss/total mass) in the mélange from $X_s = 0$ (pure amphibolite end-member) to $X_s = 1$ (pure gneissic end-member). For low gneiss fractions ($X_s < 0{\cdot}25$), the K_2O content is close to the minimum value, increasing from 0·1 wt % in the pure amphibolite ($X_s = 0$) to *c.* 4·0 wt % at $X_s = 1$. A similar variation is observed in the other major element oxides, showing a plateau in the hybrid region with no significant variations over a wide range of sediment fraction from $X_s = 0{\cdot}25$ to $X_s = 0{\cdot}75$. The CaO content of the melts from the pure gneissic end-member is very low independent of the melt fraction as indicated in previous experimental studies (Fernández *et al.*, 2008; Castro *et al.*, 2009). A small fraction of amphibolite in the composite mélange ($X_s = 0{\cdot}75$) is sufficient to increase the CaO content from 1·2 wt % ($X_s = 1$) to almost 3·0 wt % ($X_s = 0{\cdot}75$). This value remains almost constant for a wide range of mélange compositions, similar to K_2O. A summary of these coupled variations in CaO and K_2O is shown in the bottom part of Fig. 5 by plotting the mol K/(K + Ca) ratio against X_s. Granodiorite rocks characteristically have values of mol K/(K + Ca) within the range 0·3–0·8.

Projected phase relations of the experimental results are shown in Fig. 6. The results at 1100°C and 2·0 GPa for bulk compositions $X_s = 1$ (Bt-gneiss) and $X_s = 0$ (amphibolite) show contrasting three-phase assemblages, with Melt + Grt + Pl and Melt + Grt + Cpx, respectively. The compositions of the phases are also contrasted, with Ca-richer garnets and Fe + Mg + Mn-richer melts in the latter. Importantly, the mélange experiments (X_s from 0·25 to 0·75) develop a lower-variance four-phase assemblage Melt + Grt + Cpx + Pl, with intermediate phase compositions. Thus, under isothermal–isobaric conditions, clinopyroxene is lost, the grossular content of garnet decreases, and the melt changes towards a more silicic composition as the bulk-rock composition deviates from MORB amphibolite. This systematic behaviour is expected from the theory of phase equilibria. However, the change in phase composition is subtle for the assemblage

Table 2: Experimental conditions and phase compositions in mélange and isolated starting materials

Run	Ref.	Starting material	X_s	Layer/ mixture	P (GPa)	T (°C)	Assemblage[1]	Duration (h)	Phase	SiO_2	TiO_2	Al_2O_3	FeOt	MgO	MnO	CaO	Na_2O	K_2O	P_2O_5	Total	100 – total
1	AC08107-a	Gneiss	1		1·5	1000	Gl (40), Qtz (24), Grt (20),	98	Gl	72·14	0·35	16·30	1·08	0·43	0·01	0·78	2·80	5·78	0·33	100	6·4
							Spl (2), Cor (<5), Als (<5),			*0·11*	*0·02*	*0·09*	*0·06*	*0·02*	*0·02*	*0·02*	*0·03*	*0·04*	*0·06*		*0·3*
							Rt (<5)		Grt	38·03	1·21	22·07	25·99	9·43	0·5	2·43	–	–	0·31	99·97	
										0·07	*0·35*	*0·24*	*0·78*	*0·42*	*0·08*	*0·1*	–	–	*0·19*		
2	AC08111-a	Gneiss	1		1·5	1050	Gl (50), Qtz (25), Pl (15),	248	Gl	71·36	0·50	16·52	0·98	0·59	0·02	0·97	3·24	5·82	0·00	100	5·44
							Grt (5), Als (5)			*0·07*	*0·03*	*0·1*	*0·12*	*0·01*	*0·02*	*0·01*	*0·07*	*0·05*			*0·32*
									Grt	37·46	1·62	22·46	24·5	10·56	0·36	2·46	–	–	0·17	99·59	
										0·93	*0·72*	*0·68*	*1·26*	*1·03*	*0·04*	*0·19*	–	–	*0·05*		
									Pl	61·55	0·06	22·44	–	–	–	3·85	6·25	4·05	0·04	98·24	
										0·45	–	*0·51*	–	–	–	*0·69*	*0·55*	*1·4*	*0·03*		
3	AC08104	Gneiss	1		1·5	1100	Gl (82), Qtz (10), Grt (5),	200	Gl	70·82		16·72	2·09	0·92	0·01	1·36	2·96	5·12	0·00	100	5·25
							Als (3)			*0·13*	*0·05*	*0·13*	*0·1*	*0·1*	*0·01*	*0·09*	*0·03*	*0·07*			*0·07*
									Grt	38·86	0·78	22·31	21·96	13·02	0·43	1·97	–	–	0·27	99·6	
										0·28	*0·17*	*0·29*	*0·42*	*0·32*	*0·07*	*0·1*	–	–	*0·12*		
4	AC08107-b	Amphibolite	0		1·5	1000	Gl (8), Hbl + Cpx (46),	98	Gl	64·16	1·05	19·58	4·09	1·71	0·05	5·30	3·25	0·32	0·48	100	10·42
							Grt (28), Pl (18)			*0·46*	*0·07*	*0·24*	*0·08*	*0·05*	*0·02*	*0·1*	*0·08*	*0·01*	*0·04*		*0·65*
									Grt	39·18	1·05	21·61	19·88	10·06	0·68	7·48	–	–	0·08	100·02	
										0·33	*0·1*	*0·18*	*0·72*	*0·93*	*0·2*	*0·18*	–	–	*0·03*		
									Cpx	48·08	0·97	8·59	11·09	11·93	0·18	17·16	1·03	–	–	99·03	
										0·21	*0·33*	*0·6*	*0·5*	*0·1*	*0·02*	*0·17*	*0·44*	–	–		
									Pl	56·04	–	26·65	–	–	–	9·06	6·12	0·03	–	97·9	
										0·43	–	*1·02*	–	–	–	*0·21*	*0·31*	*0·04*	–		
5	AC08111-b	Amphibolite	0		1·5	1050	Gl (14), Cpx (43),	217	Gl	54·83	2·12	21·87	7·12	2·77	0·15	5·08	4·22	0·48	1·37	100	10·84
							Grt (28), Pl (14)			*0·32*	*0·06*	*0·04*	*0·12*	*0·03*	*0·02*	*0·08*	*0·34*	*0·02*	*0·08*		
									Pl	55·69	–	27·61	0·2	–	–	9	6·3	0·04	–	98·84	
										0·43	–	*1·02*	*0·23*	–	–	*0·21*	*0·31*	*0·04*	–		
									Grt	37·39	0·64	23·31	17·62	12·1	0·66	6·64	–	–	0·07	98·43	
										0·17	*0·05*	*0·42*	*0·1*	*0·09*	*0*	*0·18*	–	–	*0·01*		
									Cpx	47·26	1·81	9·74	8·6	11·69	0·19	17·86	1·72	–	0·03	98·9	
										1·21	*0·45*	*0·81*	*1·29*	*1·07*	*0·01*	*1·13*	*0·39*	–	*0·01*		
6	AC08105	Amphibolite	0		1·5	1100	Gl (52), Pl (6), Cpx (38),	200	Gl	55·66	1·57	19·65	7·1	4·22	0·15	7·03	3·99	0·23	0·4	100	7·01
						Il–Rt (<5)				*0·53*	*0·11*	*0·1*	*0·22*	*0·23*	*0·02*	*0·23*	*0·13*	*0·02*	*0·04*		*0·19*
									Cpx	45·54	1·15	11·19	9·86	11·75	0·23	16·69	1·32	0·01	–	97·74	
										0·89	*0·06*	*0·2*	*0·39*	*0·54*	*0·05*	*1·07*	*0·05*	*0·01*	–		
									Pl	55·58	–	27·3	0·2	–	–	9·8	6·01	0·04	–	98·93	
										0·41	–	*1·1*	*0·12*	–	–	*0·25*	*0·45*	*0·01*	–		

(Continued)

Table 2: Continued

Run	Ref.	Starting material	X_s	Layer/ mixture	P (GPa)	T (°C)	Assemblage[1]	Duration (h)	Phase	SiO_2	TiO_2	Al_2O_3	FeOt	MgO	MnO	CaO	Na_2O	K_2O	P_2O_5	Total	100 – total
7	AC08118-g	Gneiss	1		2·0	1100	Gl (60), Grt (22), Pl (12)	40	Gl	72·72	0·54	17·19	1·56	0·52	0·01	1·17	1·89	4·40		100	6·95
										0·04	*0·08*	*0·07*	*0·05*	*0·05*	*0·01*	*0·02*	*0·07*	*0·04*	–		*0·33*
									Grt	37·37	1·97	21·15	25·73	10·31	0·35	1·68	–	–	–	98·56	
										0·34	*0·73*	*0·45*	*0·39*	*0·49*	*0·11*	*0·43*	–	–	–		
									Pl	61·71	0·03	22·07	0·12	0	0·01	3·82	7·24	1·66	–	96·66	
										0·8	*0·02*	*0·7*	*0·04*	*0·01*	*0·01*	*0·65*	*0·41*	*0·78*	–		
8	AC08118-p	Amphibolite	0		2·0	1100 Hbl (8)	Gl (22), Grt (30), Cpx (40),	40	Gl	65·79	1·87	20·09	4·86	1·51	0·06	4·63	1·03	0·16		100	11·71
										0·69	*0·15*	*0·3*	*0·07*	*0·34*	*0·01*	*0·5*	*0·05*	*0·01*	–		*0·85*
									Grt	38·09	1·86	20·79	18·26	10·91	0·47	7·63	–	–	–	98·01	
										0·25	*0·28*	*0·18*	*0·28*	*0·18*	*0·05*	*0·09*	–	–	–		
									Cpx	46·2	1·57	11·78	8·57	9·41	0·12	17·95	2·25	–	–	97·85	
										0·38	*0·12*	*0·4*	*0·18*	*0·36*	*0·01*	*0·29*	*0·2*	–	–		
									Hbl	46·41	0·95	8·87	13·37	12·56	0·23	12·87	1·35	0·01	–	96·62	
										0·11	*0·18*	*0·05*	*0·11*	*0·24*	*0·02*	*0·16*	*0·02*	*0·01*	–		
9	AC08100	Mélange	0·5	Layers	1·5	1000	Gl (40), Grt (20), Pl (20),	88	Gl	72·73	0·49	16·06	1·33	0·49	0·01	1·62	2·64	4·62	0·00	100	6·05
							Cpx (10), Hbl (5), Opx			*0·36*	*0·05*	*0·12*	*0·22*	*0·05*	*0·01*	*0·25*	*0·08*	*0·11*			*0·37*
							(<5), Rt (<5)		Grt	37·87	1·44	21·31	22·02	9·09	0·41	5·47	–	–	0·18	97·79	
										0·55	*0·35*	*0·45*	*2·59*	*1·48*	*0·22*	*2·63*	–	–	*0·09*		
									Opx	49·37	0·27	4·45	21·59	19·31	0·26	1·43	0·15	–	0·02	96·85	
									Hbl	49·1	0·94	8·1	9·42	12·81	0·14	14·92	1·36	–	0·05	96·84	
									Pl	59·78	–	25·87	–	–	–	7·62	6·57	1·24	–	101·08	
										3·44	–	*2·2*	–	–	–	*2·73*	*1·01*	*0·85*	–		
									Cpx	48·77	1	9·23	9·16	11·32	0·09	17·39	1·64	–	0·07	98·67	
										0·01	*0·04*	*0·33*	*0·3*	*0·37*	*0*	*0·48*	*0·14*	–	*0*		
10	AC08109	Mélange	0·5	Layers	1·5	1050	Gl (50), Grt (20), Opx (5),	228	Gl	70·87	0·81	15·94	2·66	0·73	0·02	2·19	2·39	4·09	0·29	100	6·37
							Cpx (25)			*0·4*	*0·13*	*0·12*	*0·25*	*0·06*	*0·01*	*0·21*	*0·16*	*0·26*	*0·06*		*0·35*
									Cpx	47·98	1·21	8·68	10·36	12·32	0·15	16·7	1·09	–	0·03	98·52	
										2·13	*0·5*	*3·36*	*0·19*	*1·05*	*0·01*	*0·74*	*0·1*	–	*0·02*		
									Opx	50·1	0·38	5·28	18·98	22·55	0·21	1·39	0·13	–	0·02	99·04	
										1·15	*0·13*	*1·43*	*1·61*	*1·95*	*0·05*	*0·16*	*0·02*	–	*0*		
11	AC08103	Mélange	0·5	Layers	1·5	1100	Gl (80), Opx (14), Pl (4),	240	Gl	65·43	1·19	17·47	2·88	1·96	0·09	4·50	2·99	3·23	0·27	100	6·5
							Cpx (<5)			*1·25*	*0·15*	*0·39*	*0·3*	*0·28*	*0·03*	*0·43*	*0·15*	*0·18*	*0·04*		*0·32*
									Opx	50·93	0·36	5·8	14·61	25·08	0·29	1·39	0·08	–	0·02	99	
										2·29	*0·17*	*2·74*	*2·77*	*2·85*	*0·04*	*0·1*	*0·02*	–	*0·01*		
									Cpx	50·13	0·82	6·28	6·88	14·58	0·18	18·53	0·71	0·04	0·02	98	
									Pl	55·06	–	27·66	0·25	–	–	9·9	5·05	0·56	–	98	

(Continued)

Table 2: Continued

Run	Ref.	Starting material	X_s	Layer/ mixture	P (GPa)	T (°C)	Assemblage[1]	Duration (h)	Phase	SiO_2	TiO_2	Al_2O_3	FeOt	MgO	MnO	CaO	Na_2O	K_2O	P_2O_5	Total	100 – total
12	AC08102	Mélange	0·5	Layers	1·5	1200	Gl (100)	75	Gl	62·42	16·19	5·79	4·35	0·09	5·77	2·93	2·46	0·00	100		
										0·32	*0·06*	*0·18*	*0·07*	*0·07*	*0·02*	*0·07*	*0·02*	*0·04*			
13	AC08120a	Mélange	0·25	Mixture	1·5	1100	Gl (75)[2]	150	Gl	56·32	2·03	17·41	6·44	4·53	0·00	7·62	4·03	1·63	0·00	100	
										0·12	*0·01*	*0·04*	*0·15*	*0·04*	*0*	*0·15*	*0·13*	*0·06*			
14	AC08120b	Mélange	0·75	Mixture	1·5	1100	Gl (70)[2]	150	Gl	65·65	0·93	16·83	2·70	2·59	0·03	3·66	3·79	3·84	0·00	100	
										0·41	*0·18*	*0·28*	*0·42*	*0·26*	*0·06*	*0·13*	*0·3*	*0·21*			
15	AC08114	Mélange	0·25	Layers	2·0	1100	Gl (60), Grt (5), Cpx (25), Pl (10)	228	Gl	69·15	1·07	16·54	2·49	0·83	0·02	3·04	3·33	3·51		100	6·05
										0·69	*0·08*	*0·17*	*0·22*	*0·09*	*0·02*	*0·19*	*0·11*	*0·11*	–		*0·37*
									Grt	38·83	2·13	21·23	19·1	10·71	0·43	7·32	–	–	–	99·75	
										0·1	*0·23*	*0·13*	*1·33*	*0·88*	*0·05*	*2·26*	–	–	–		
									Cpx	47·8	1·4	12·1	8·2	10	0·1	17·2	2	–	–	98·8	
										1·9	*0·2*	*2·6*	*0·5*	*1·2*	*0·0*	*0·7*	*0·1*	–	–		
									Pl	60·61	–	24·06	0·28	–	–	5·82	6·76	0·94	–	98·47	
										1·56	–	*1·45*	*0·12*	–	–	*0·56*	*1·12*	*0·23*	–		
16	AC08119	Mélange	0·5	Layers	2·0	1100	Gl (65), Grt (15), Cpx (10), Pl (5), Hbl (<5), Qtz (<5), Rt (<5)	140	Gl	65·70	1·02	16·72	2·03	2·32	0·02	4·96	4·13	3·11	0·00	100	6·79
										0·15	*0·24*	*0·27*	*0·1*	*0·22*	*0·03*	*0·07*	*0·04*	*0·08*			*0·79*
									Pl	60·65	–	23·5	0·78	–	–	5·74	7·02	1·12	–	98·81	
										1·75	–	*1·65*	*0·03*	–	–	*0·71*	*1·02*	*0·13*	–		
									Grt	38·3	1·75	21·67	22·02	12·12	0·31	3·11	–	–	0·16	99·44	
										0·59	*0·5*	*0·53*	*1·24*	*0·6*	*0·04*	*0·32*	–	–	*0·04*		
									Cpx	47·39	1·23	12·14	8·44	9·73	0·08	17·29	2·06	–	0·05	98·41	
									Hbl	48·03	0·75	9·28	16·24	16·27	0·25	6·63	0·9	–	0·09	98·44	
17	AC08116	Mélange	0·75	Layers	2·0	1100	Gl (70), Grt (20), Cpx (5), Pl (5)	240	Gl	69·94	0·82	15·98	2·04	1·02	0·02	2·80	2·94	4·43		100	5·62
										0·04	*0·06*	*0·04*	*0·08*	*0·03*	*0·01*	*0·07*	*0·02*	*0·11*	–		*0·27*
									Cpx	49·98	0·88	8·09	7·87	13·3	0·11	16·67	1·33	–	–	98·23	
										0·1	*0·06*	*0·23*	*0·54*	*0·17*	*0·04*	*0·59*	*0·06*	–	–		
									Grt	38·93	2·05	21·24	19·61	11·25	0·4	5·58	–	–	–	99·06	
										0·25	*0·32*	*0·16*	*0·97*	*0·61*	*0·05*	*1·34*	–	–	–		
									Pl	60·9	–	23·74	0·19	0·02	0·02	5·83	6·29	1·45	–	98·44	
										2·28	–	1·37	0·14	–	–	1·41	0·69	0·19	–		

Average values in wt % oxides for a total number of analyses from four to 10 points in glass and minerals. Standard deviations (1σ) in italics. Water content in all runs is the water coordinated in hydrous minerals. amphibole and micas. This is reported in Table 1. —, abundances below detection limit. X_s, weight fraction of sediment (mica-rich gneiss) in the mélange.

[1]Mineral abbreviations from Kretz (1983). Als, Al-silicate; Rt, rutile; Gl, glass (quenched melt). Numbers in parentheses in the assemblages are approximate modal abundances estimated by image analyses on backscattered electron images. Low modal abundances are reported as <5.

[2]In homogeneous mixtures only glass compositions are reported because of the small size of the crystals.

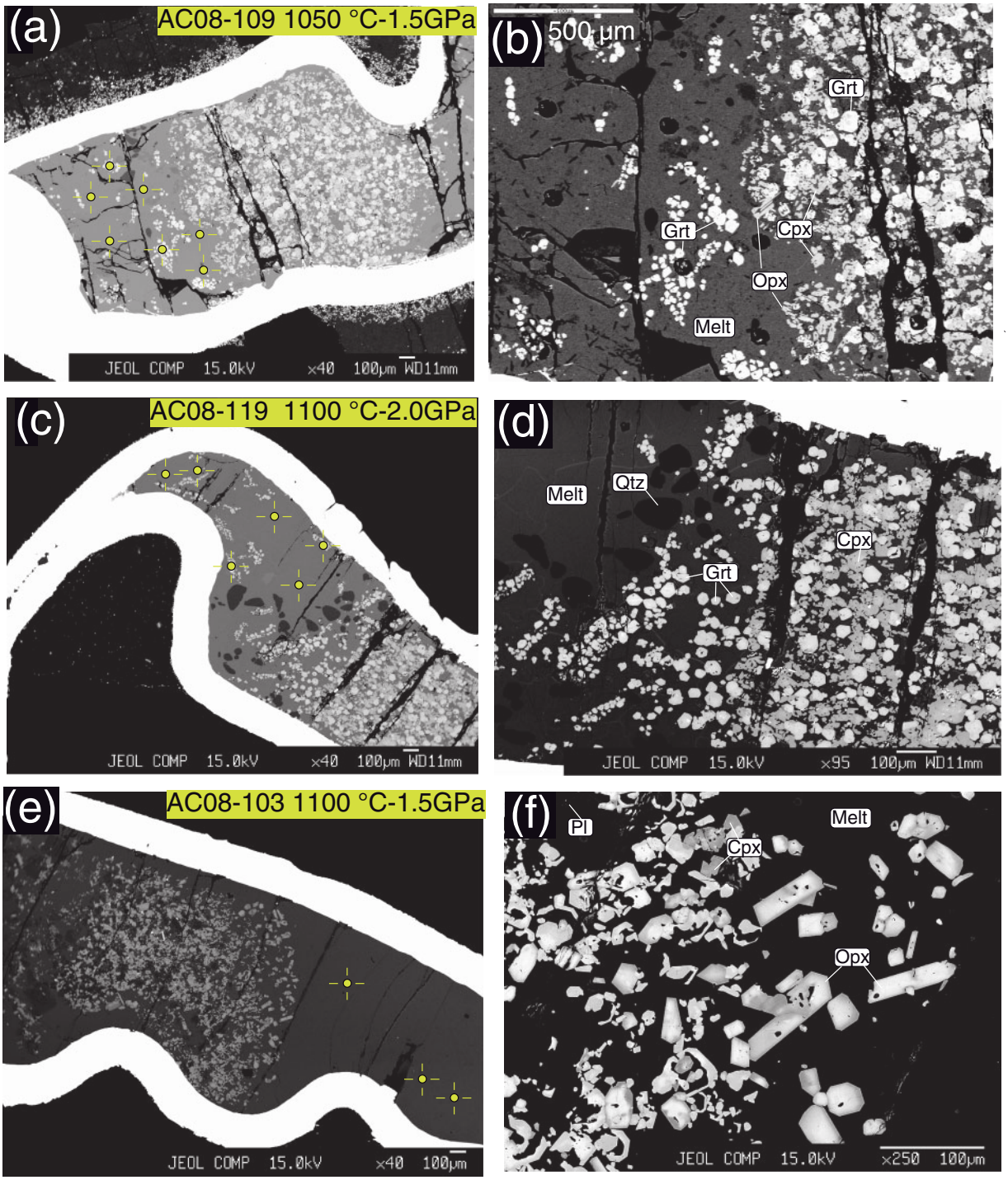

Fig. 3. Back-scattered electron images of representative run products from composite capsules simulating a multilayer mélange: (a, c, e) general views of the experimental capsules; (b, d, f) respective details of the interface between adjacent layers. It should be noted that the interface is marked by an abrupt change in the modal proportions of minerals, recording the original compositional differences between the layers. Crosses in images in the left column show the position of LA-ICP-MS analyses. Several laser holes are shown in (b) as black circles

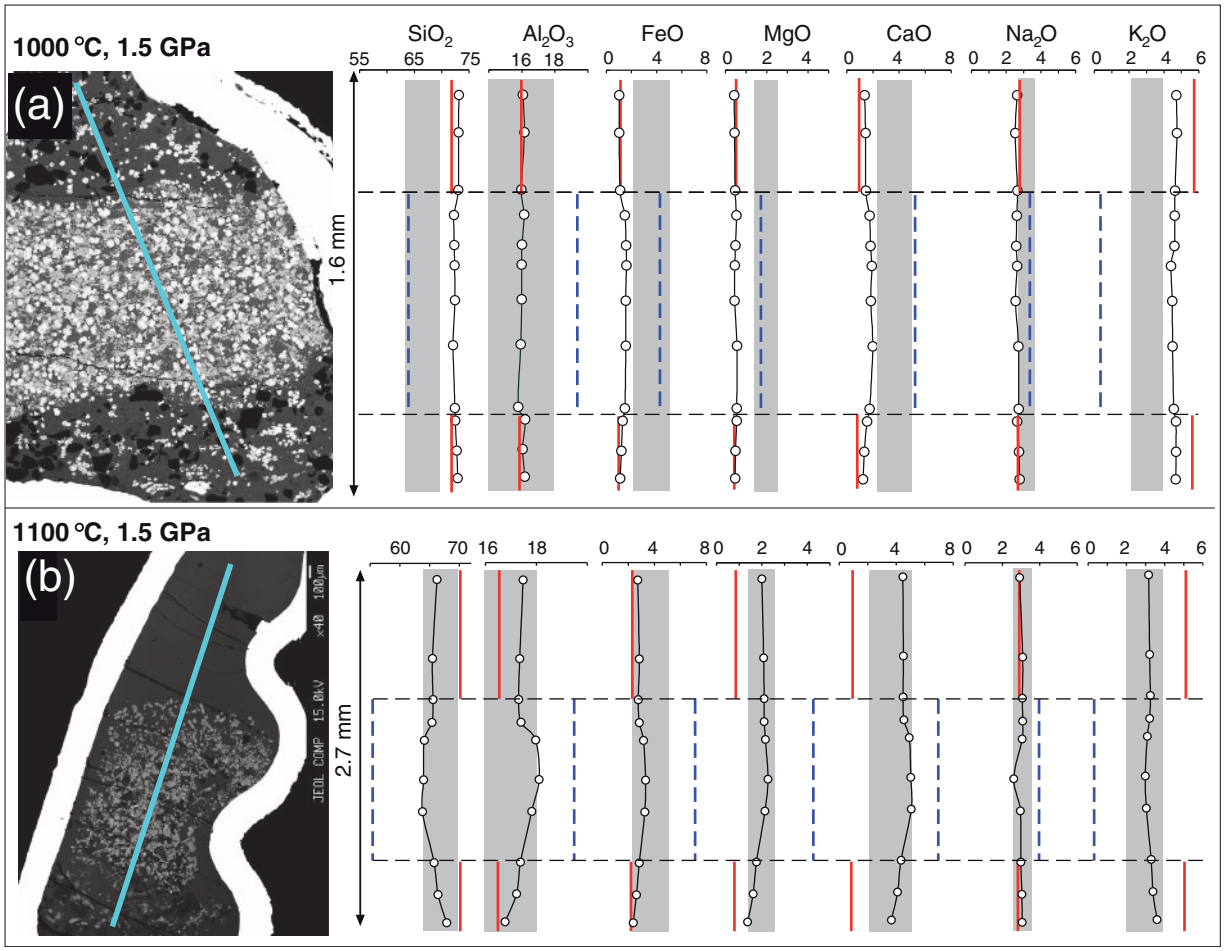

Fig. 4. Compositional profiles of melts (quenched glass) in two runs with composite capsules at 1000 and 1100°C (1·5 GPa). The coexisting mineral assemblage is dominated by Qtz–Grt–Px–Pl at 1000°C and by Px–Pl at 1100°C. Noteworthy features are the homogeneous compositions of the melts across the layers and the hybrid composition of these melts compared with melts derived from the pure end-members. These are represented by bold continuous lines (red) for the gneiss end-member, and by bold dashed lines (blue) for the amphibolite end-member. The grey band represents the compositional range for Cordilleran granodiorite–tonalite rocks from the Peninsular Ranges and Sierra Nevada batholiths in North America (Lee *et al.*, 2007). Only rocks within the silica range 63–70 were considered in this selection. It should be noted that melts at 1100°C fit this compositional range for all major elements. At 1000°C the melts are out of this range for most elements.

Grt + Cpx + Pl + Melt, even if it formed from contrasted bulk-rock compositions such as $X_s = 0{\cdot}25$ and $X_s = 0{\cdot}75$, indicating the buffering capability of this lower-variance assemblage. This result is clearly illustrated by the almost identical composition of the melts. Results at 1·5 GPa with the same starting materials and at the same temperature of 1100°C show a similar buffering effect for the liquid compositions. However, the fraction of gneiss is more restricted (X_s from 0·5 to 0·75) compared with the results at 2·0 GPa. The melt produced at 1·5 GPa and 1100°C is not buffered, with $SiO_2 = 56{\cdot}3$ wt %, below the lower limit (63 wt %) characteristic of granodiorites and tonalites. The other mélange compositions with $X_s = 0{\cdot}5$–$0{\cdot}75$ produced buffered melts with very similar compositions (runs 11 and 14 in Table 2). According to these results, the buffering effect is more marked at 2·0 GPa.

An interesting result was the change in the composition of the melts obtained at variable temperatures and constant pressure from a particular mélange composition (X_s = constant). These changes are systematic and demonstrate that our runs reached equilibrium. They also indicate the effect of temperature on magma composition as a response to variable coexisting solid phase assemblages. Figure 7 shows these changes for runs at $P = 1{\cdot}5$ GPa and T from 1000°C to 1200°C. Although the proportions of the gneiss and amphibolite components are constant in all these runs ($X_s = 0{\cdot}5$), the compositions of hybrid melts show important differences. This is due to the control

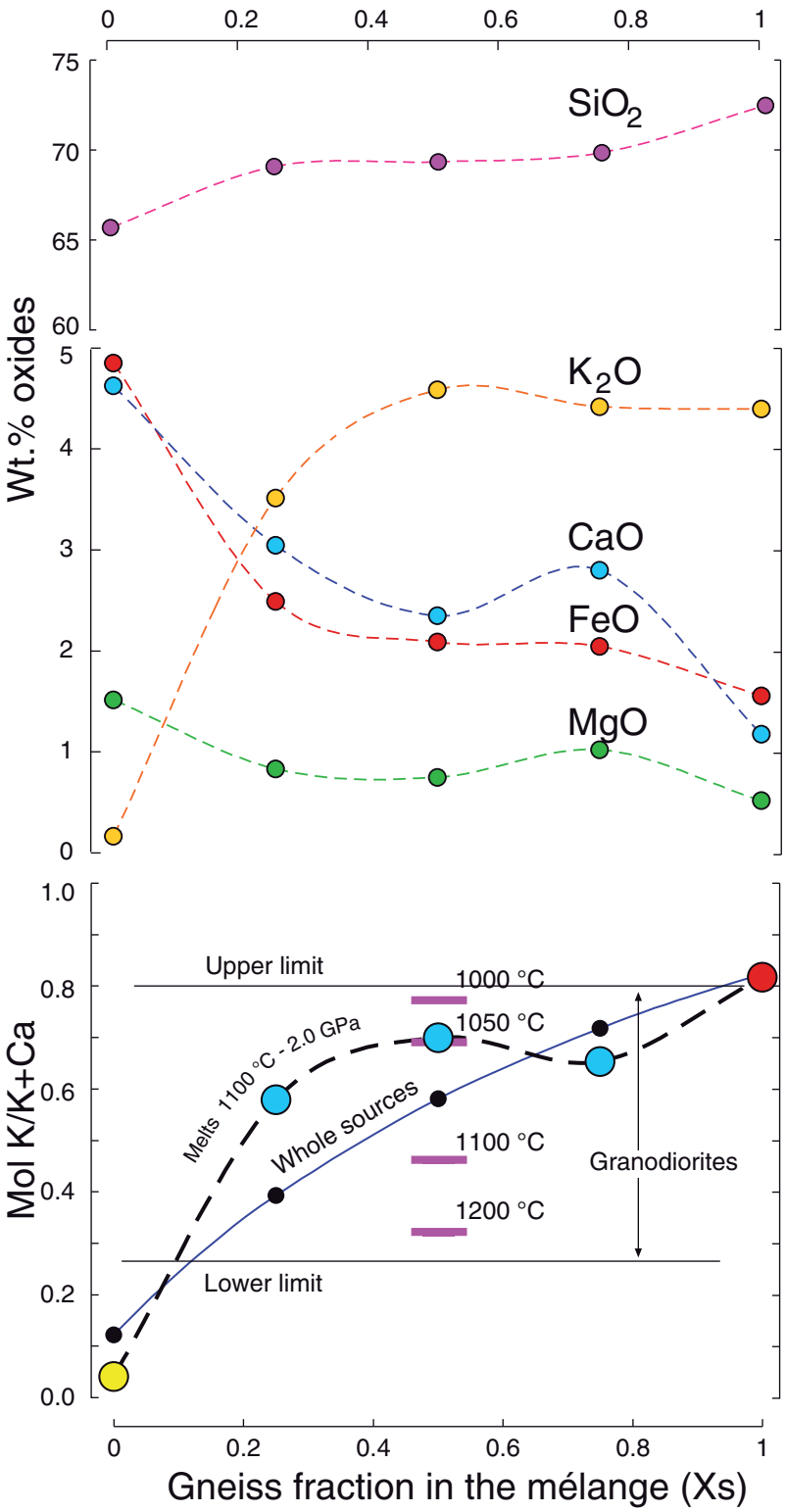

Fig. 5. Variations of melt composition as a function of the fraction of sediment in the composite mélange at constant pressure (2·0 GPa) and temperature (1100°C). The composition of melts from mélanges with low (25%) to high (75%) fractions of sediment does not vary significantly. The data define a plateau for the most abundant major elements (Al, Si, Ca, Fe, Mg, Na, K). These results indicate the buffering effect of the co-existing mineral assemblage.

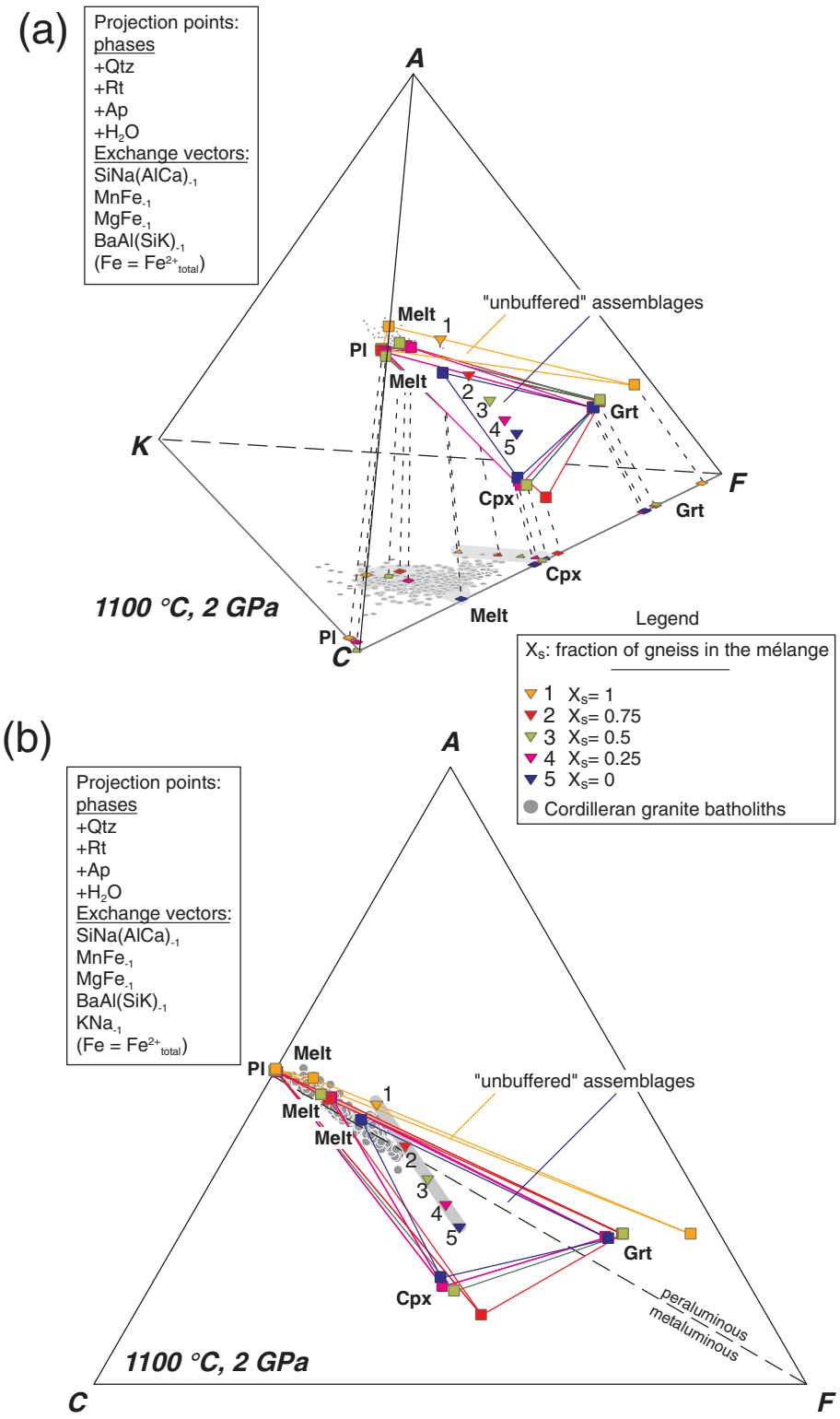

Fig. 6. (a) Condensed AKCF and (b) ACF diagrams for the experimental results at 1100°C and 2 GPa constructed after projection of the compositions of the studied starting bulk-rock compositions (triangles), experimental mineral and melts (squares), and natural granitic rocks (grey circles) from the indicated phases and exchange vectors, with indication of 'buffered' and 'unbuffered' phase assemblages. In (b), a line of ASI = 1·0 is plotted for reference (dashed line). It should be noted that feldspar components are collinear in the AKCF (and ACF) diagrams because of projection through the exchange vectors $AlCa(SiNa)_{-1}$ and NaK_{-1}.

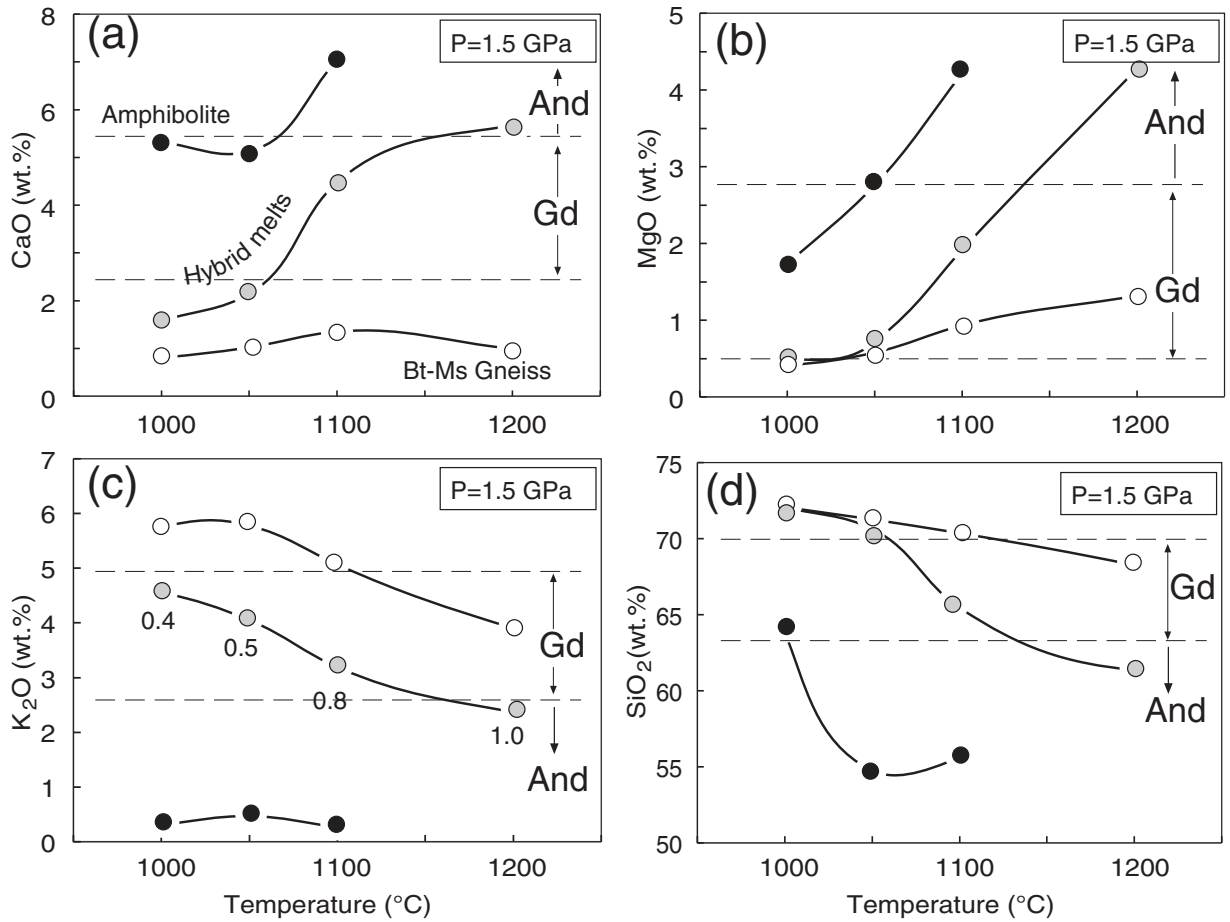

Fig. 7. Variations of melt composition as a function of temperature for a constant composition (mélange of 50% gneiss and 50% amphibolite) at 1·5 GPa pressure. The compositions of melts from the end-member materials of the mélanges, amphibolite (black circles) and gneiss (white circles), at the same P–T conditions are also shown. At $T < 1100^{\circ}C$ the increments in CaO (a) and MgO (b) with respect to the gneiss melt baseline are small compared with the large enrichments in these elements at $T \geq 1100^{\circ}C$. Melt fractions in composite capsules are indicated. Dashed lines represent the range of typical granodiorite and tonalite Cordilleran-type plutonic rocks within the silica range 63–70 wt % from the Sierra Nevada and Peninsular Ranges batholiths (Lee *et al.*, 2007).

imposed by the coexisting mineral assemblage and, hence, by the temperature. The variation in K_2O (Fig. 7c) follows a distinct trend with a good proportionality with respect to the composition of the gneiss baseline. The decrease in K_2O with increasing T is due to its dilution in the melt as the increasing melt volume reduces the weight proportion in the system. This differential behaviour with respect to other components is due to the absence of any K-bearing coexisting crystalline phase. The behaviour of SiO_2 (Fig. 7d) is anticorrelated with that of MgO (Fig. 7b), indicating the strong control of temperature and coexisting minerals on the composition of the hybrid melts.

Gravitational settling of crystals was observed in most composite capsule runs (Fig. 3). These were selected for LA-ICP-MS trace element analysis. Average melt compositions are given in Table 3 for three selected experimental runs. The small size of Grt, close to the 30 μm diameter of the laser beam, made it difficult to obtain point analyses devoid of contamination from the surrounding glass. However, a good approximation was obtained by recasting the mixed analyses (Grt + glass) to the proportion of Grt to glass in the mixture. This proportion was obtained by linear regression of selected elements, not coordinated in the Grt structure, and the measured abundance of the same elements in the surrounding melt. The best correlation (Pearson's coefficient >0·99) was found for the group of elements Li, Be, Rb, Sr and Ba; these were therefore used to estimate the proportion of contaminant in the mixed analyses. The results after discounting the contamination are given in Table 3, together with the calculated Grt/melt partition coefficients (K_d). It should be appreciated that melts produced in equilibrium with Grt are strongly heavy rare earth element (HREE) fractionated

Table 3: Laser ablation trace element compositions of melts and coexisting garnets from composite mélanges

Run:	AC08-109				AC08-103		AC08-113			
P:	1·5 GPa				1·5 GPa		2·0 GPa			
T:	1050°C				1100°C		1100°C			
	Melt[1] ($n=3$)	SD	Grt[2]	K_d	Melt ($n=3$)	SD	Melt ($n=4$)	SD	Grt[2]	K_d
Li	43·4	1·6	—	—	42·7	1·6	42·9	4·7	—	—
Be	2·3	0·1	—	—	2·9	0·0	2·2	0·2	—	—
V	39·7	0·3	357·2	12·6	92·1	1·3	51·8	4·5	179·0	4·8
Cr	5·6	0·7	827·2	206·1	30·6	1·9	5·8	2·3	664·1	159·6
Co	10·0	0·7	153·4	21·4	7·4	0·2	10·2	1·2	133·4	18·4
Ni	1·0	0·3	24·1	33·9	0·6	0·1	2·7	0·3	21·9	11·5
Cu	0·8	0·2	2·2	3·7	0·7	0·6	0·9	0·2	16·0	24·3
Zn	136·3	3·0	335·5	3·4	18·5	1·1	33·7	4·4	86·0	3·6
Rb	181·2	5·3	—	—	143·1	9·2	169·5	11·9	—	—
Sr	120·3	2·9	—	—	183·8	7·7	165·7	12·7	—	—
Y	16·8	0·4	68·6	5·7	47·9	3·1	14·5	1·7	57·4	5·5
Zr	88·7	6·3	59·3	0·9	253·3	7·7	109·3	10·7	20·3	0·3
Nb	7·6	0·6	27·4	5·1	7·9	0·2	8·6	1·0	11·6	1·9
Cs	6·8	0·2	1·8	0·4	5·6	0·2	6·8	0·5	0·4	0·1
Ba	763·5	20·1	—	—	788·4	22·2	727·6	70·9	—	—
La	33·2	0·8	3·4	0·1	38·9	0·6	32·2	3·3	4·1	0·2
Ce	67·2	0·9	10·2	0·2	69·8	3·3	64·6	6·4	14·8	0·3
Pr	7·1	0·2	2·2	0·4	8·5	0·2	6·7	0·7	2·3	0·5
Nd	29·4	1·3	26·0	1·2	37·8	0·4	27·3	1·9	20·1	1·0
Sm	6·0	0·2	15·2	3·5	9·2	0·8	5·0	0·6	8·8	2·5
Eu	1·1	0·1	2·9	3·9	2·1	0·1	0·9	0·0	1·9	3·0
Gd	4·5	0·2	15·5	4·8	9·0	0·9	3·9	0·5	8·6	3·1
Tb	0·6	0·0	2·3	5·4	1·5	0·1	0·5	0·1	1·5	3·9
Dy	3·5	0·2	14·5	5·9	8·7	0·8	2·7	0·4	9·6	5·0
Ho	0·6	0·1	2·6	5·9	1·8	0·1	0·5	0·1	2·2	5·9
Er	1·6	0·1	7·5	6·7	5·0	0·3	1·3	0·2	6·8	7·6
Tm	0·2	0·0	0·9	5·7	0·7	0·0	0·2	0·0	1·0	8·4
Yb	1·3	0·1	5·6	6·0	4·3	0·3	1·0	0·2	6·1	8·7
Lu	0·2	0·0	0·8	6·3	0·7	0·0	0·2	0·0	1·1	10·1
Hf	2·8	0·5	1·1	0·6	6·8	0·1	3·0	0·3	0·4	0·2
Ta	0·7	0·1	1·8	3·6	0·7	0·0	0·6	0·0	1·1	2·4
Tl	1·1	0·1	0·1	0·2	0·1	0·0	0·1	0·0	0·1	1·0
Pb	29·1	1·2	4·4	0·2	0·3	0·0	0·6	0·1	0·7	1·6
Th	12·0	0·2	1·2	0·1	12·2	0·4	10·6	0·7	1·8	0·2
U	4·2	0·1	1·3	0·4	3·6	0·2	3·8	0·2	1·3	0·5

[1]Abundances in ppm normalized to 70 wt % silica in AC08-109 and AC08-113, and to 65 wt % silica in AC08-103.
[2]Garnet compositions calculated by mass balance from mixed melt–garnet analyses (see text).

compared with melts in equilibrium with a Grt-free mineral assemblage. Figure 8 shows MORB-normalized and chondrite-normalized (REE) variation diagrams for incompatible elements determined in the experimental glasses at the conditions of 1050–1100°C, 1·5 GPa and 1100°C, 2·0 GPa. These patterns are consistent with the expected behaviour of incompatible elements in silicate magmas. The comparison with natural rocks is discussed below.

DISCUSSION

Our experimental results indicate that partial melting of a composite source in subduction zone environments is an effective mechanism to produce hybrid melts of granodiorite composition. Previous experimental studies with composite basalt–crust starting materials (Patiño-Douce, 1995; Castro *et al.*, 1999) were aimed at investigating the behaviour of composite systems in assimilation processes. Although these experiments were performed at crustal

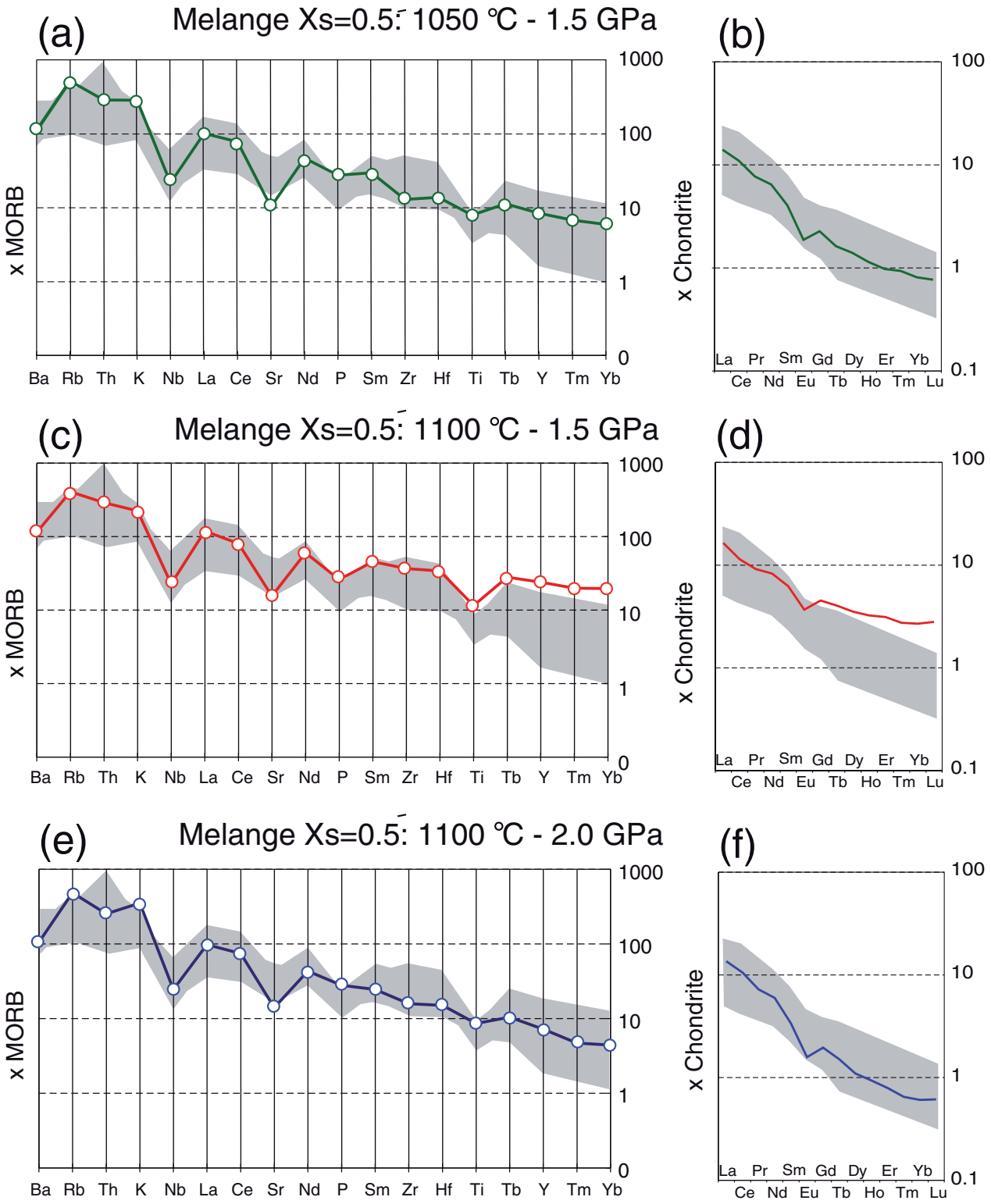

Fig. 8. MORB-normalized incompatible element and chondrite-normalized REE patterns for experimental glasses in equilibrium with Grt (a, b, e, f) and in a Grt-free assemblage (c, d). Shaded areas represent the range of Cordilleran granodiorites from the Peninsular Ranges batholith (Lee *et al.*, 2007).

pressures (0·6–1·0 GPa), they produced interesting results that can be applied both to processes of crustal assimilation and to shallow-level mélange melting. The experimental results presented here are a continuation of these previous studies at conditions more appropriate for lithosphere mantle depths (1·5–2·0 GPa) at which mantle wedge plumes are underplated, according to the numerical thermomechanical simulations (Fig. 2). We evaluate these new experimental results to test the plume-to-batholith model in three important respects: (1) the comparison of melt compositions with those of typical Cordilleran-type batholiths; (2) the feasibility for homogenization of melts; (3) the plausibility of generating relatively homogeneous granodiorite–tonalite melt compositions from heterogeneous sources.

The comparison of experimental hybrid melts with batholiths

Experimental melts from composite mélanges in the temperature range 1050–1100°C are silicic ($SiO_2 > 63$ wt %), consistent with the compositional range of the granodiorites to tonalites that form more than 90 vol. % of Cordilleran-type batholiths (see below). This composition is more dependent on temperature than the proportions of basaltic and gneissic components in the mélange (Fig. 5). Melts developed at 1000°C are too silicic, falling outside the range of the most important major elements characteristic of granodiorites and tonalites (Figs 4 and 7). The experimental melts are poor in Ca, Fe and Mg, below the lower limit of granodiorites and tonalites. Melts of the pure end-members are also out of range at any temperature. At 1200°C the melt fraction approaches total melting and, consequently, the composition of the melt approaches that of the mixed source, which is, in broad terms, andesitic (Table 1). The MORB-normalized trace element patterns of the experimental melts at 1050°C, 1·5 GPa and 1100°C, 2·0 GPa (Grt-present) are almost coincident with the field of Cordilleran-type batholiths (Fig. 8). Significant negative anomalies (e.g. Nb, Sr, Ti) in the trace element patterns of the batholiths are fairly well reproduced by the experimental melts in these MORB-normalized diagrmas. It should be noted that rutile was identified forming large (>50 μm) polycrystalline aggregates in several of the experimental runs with composite capsules (Table 2). This textural distribution explains why rutile was not always identified in thin section. This mineral may be responsible for the observed depletion in Nb and Ti in the analyzed glasses. The Grt-absent experiment at 1100°C and 1·5 GPa also shows a melt composition coincident with the trace element pattern of Cordilleran batholiths, with the exception of the HREE, which are not depleted in comparison with the batholiths. The chondrite-normalized REE patterns for the experimental melts are also consistent with those of the batholiths, with the exception of the Grt-free experiment (Fig. 8d). Thus, we conclude that the incompatible-element budget for Cordilleran batholiths could be explained by partial melting at high T (1050–1100°C) of a composite mélange comprising subducted basalt (MORB) and sediment in variable proportions.

Figure 9 shows a comparison, in terms of major elements, between the experimental melts and Cordilleran-type granitoid rocks from the North America active continental margin. Most hybrid melts formed from composite mélanges at 1100°C and 1·5–2·0 GPa plot within a small field on these diagrams that overlaps with the composition of more than 90 vol. % of the outcropping plutonic rocks in Cordilleran batholiths (i.e. granodiorites and tonalites). The Coastal Batholith of Peru, which intruded the continental margin of South America from mid-Cretaceous to Neogene times, shows an area percentage of tonalite and granodiorite rocks ranging from 84 to 93% (see compilation by Cobbing *et al.*, 1981), but only 7–10% of mafic rocks (gabbro and diorite), and minor amounts of leucogranitic plutons. Similar proportions are estimated for the Coastal Batholith of Canada. Planimetry of cumulative areas of felsic, intermediate and mafic plutons represented on a detailed geological map of the British Columbia (Massey *et al.*, 2005) shows that tonalite and granodiorite represent an area fraction of around 91%, with subordinate gabbro and diorite (~7%) and leucogranite plutons (~2%). Composition–size–depth relationships for Mesozoic intrusions of the western USA presented by Barton *et al.* (1991) suggest that the relative area of gabbro and diorite lithologies is less than 25% across the entire Cordilleran crust of North America, although mafic compositions may be more abundant in the lowermost crust. More recent data by Ducea (2001) for the California active margin (from ~220 to ~80 Ma) indicate that upper crustal exposures are ~97% tonalitic and granodioritic with <3% mafic intrusions. Mid-crustal exposures show similar proportions within a very thick (up to 30–35 km) mostly granodiorite–tonalite batholith (Ducea, 2001). In summary, magmas of intermediate composition (tonalites and granodiorites) appear to be the main product of subduction-related Cordilleran magmatic arcs; a consistent proportion (~90%) is observed in western North America (Coastal Batholith of Canada, Sierra Nevada and Peninsular Ranges Batholiths) and South America (Coastal Batholith of Peru).

Other compositions, either more mafic (diorites and gabbros) or more felsic (granites *sensu stricto*) are also present in Cordilleran-type plutonic associations (Fig. 9). The more silicic members may represent low-temperature melts. Diorites may represent either extremely high-temperature (~1200°C) melts, developed from the same source as the granodiorites and tonalites, or by-products of reaction of silicic melts with the peridotite mantle (Kelemen, 1995; Kelemen *et al.*, 2003). Gabbroic rocks

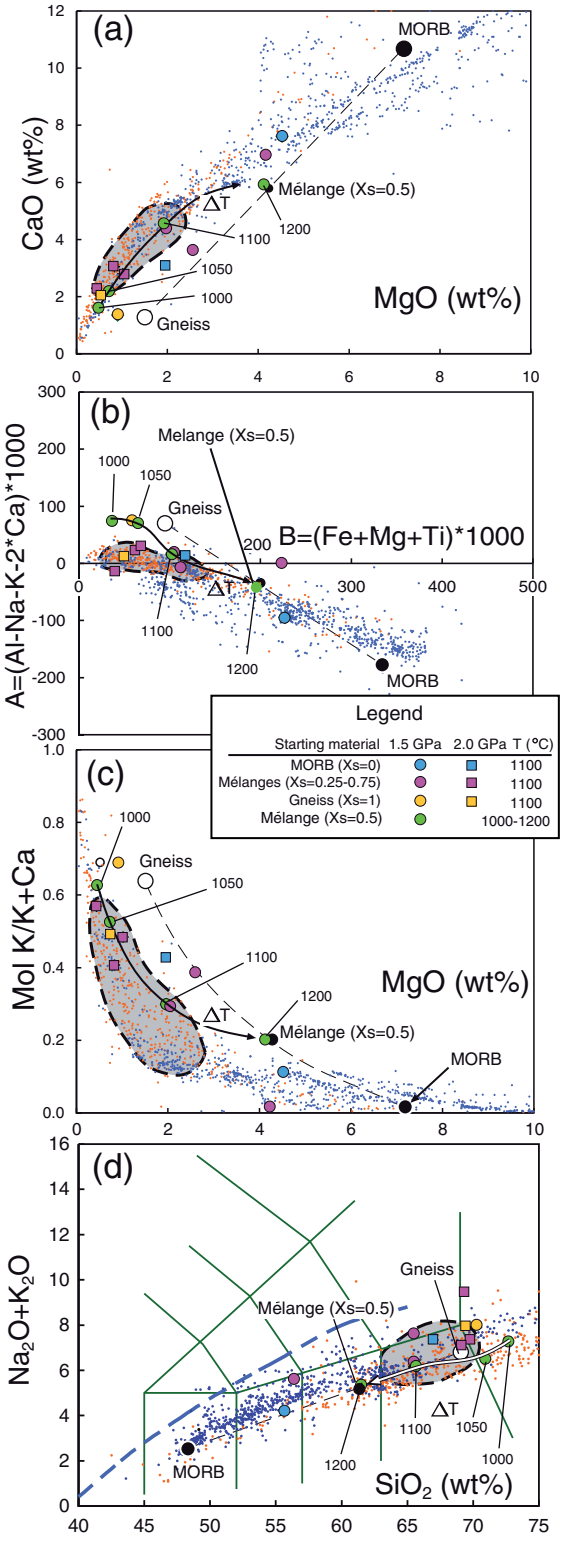

Fig. 9. Comparisons of experimental melts derived from composite mélanges and the compositional variation of typical Cordilleran-type batholiths (red dots; Peninsular Ranges and Sierra Nevada) and andesites (blue dots; Cascades) from North America. It should be noted that the experimental melts plot within the field of the natural magmatic rocks. The buffered compositions at 1100°C and 1·5–2·0 GPa plot within the encircled areas (dashed bold line) of the diagrams, which represent more than 90 vol. % of the outcropping plutonic rocks in Cordilleran-type batholiths (see text). The variable melt compositions, produced at T from 1000 to 1200°C, display a trend (large arrow labelled ΔT) coincident with the general array of Cordilleran-type rocks. The two end-members, MORB (amphibolite) and Bt-gneiss, are also plotted in the diagrams, together with a mixing line representing the source of the batholiths. The point $X_s = 0{\cdot}5$ represents a mélange with equal proportions of amphibolite and gneiss. Total melting of this mélange gives a typical andesitic liquid. The melts from isolated end-members, namely MORB and Bt-gneiss, are out of the range of common Cordilleran-type batholiths, indicating that both end-member components are needed for the generation of the magmas. Data from Sierra Nevada and Peninsular Ranges are taken from Lee *et al.* (2007). Data for the Cascades correspond to lavas from Medicine Lake, Mt. Shasta, Mt. St. Helens and Mt. Larsen, taken from the compilation in the GEOROC database (http://georoc.mpch-mainz.gwdg.de/georoc/).

represent less than 2 vol. % in Cordilleran batholiths. These are probably derived from a metasomatized mantle source by processes of fluid-fluxed melting (Grove *et al.*, 2005). These compositions are predicted in the plume model discussed here and in previously published numerical experiments (e.g. Gerya & Yuen, 2003*b*).

Similar comparisons are evident in terms of trace element characteristics. The presence of Grt in the source region has an important effect on the HREE/LREE (light REE) ratio in the coexisting melt. In general, depletion in HREE in mantle-derived magmas is directly related to the depth of magma generation, as a result of the pressure-dependent stability of Grt. However, at near-liquidus conditions below 2·3 GPa, Grt is not stable in systems with the composition of the mélanges used in our experimental study [e.g. the andesite of Green (1982, fig. 7); Table 1].

Figure 10 shows a comparison of the REE abundances in our experiments and in the Cordilleran batholiths of the American active continental margin. Experimental melts in equilibrium with Grt are characterized by strong REE fractionation with $Ce_N/Yb_N > 10$ and $Yb_N < 10$. Granodiorites from the Peninsular Ranges batholith in North America and the Patagonian batholith in South America exhibit a wide spectrum of REE patterns from strongly fractionated to unfractionated. Some granodiorites in these batholiths plot in the Grt-free region of the diagram, whereas many others appear to be produced from a source in equilibrium with Grt. Slight differences in the P and/or T of melting may be the cause of these variations if the source region is at P–T conditions close to the upper stability limit of Grt. Interestingly, these wide differences in REE patterns are in marked contrast to the narrow range in major-element composition, reinforcing the idea of a buffering effect of the coexisting mineral assemblage on the major element compositions. In general, the REE data (Fig. 10) for the batholiths follow a trend

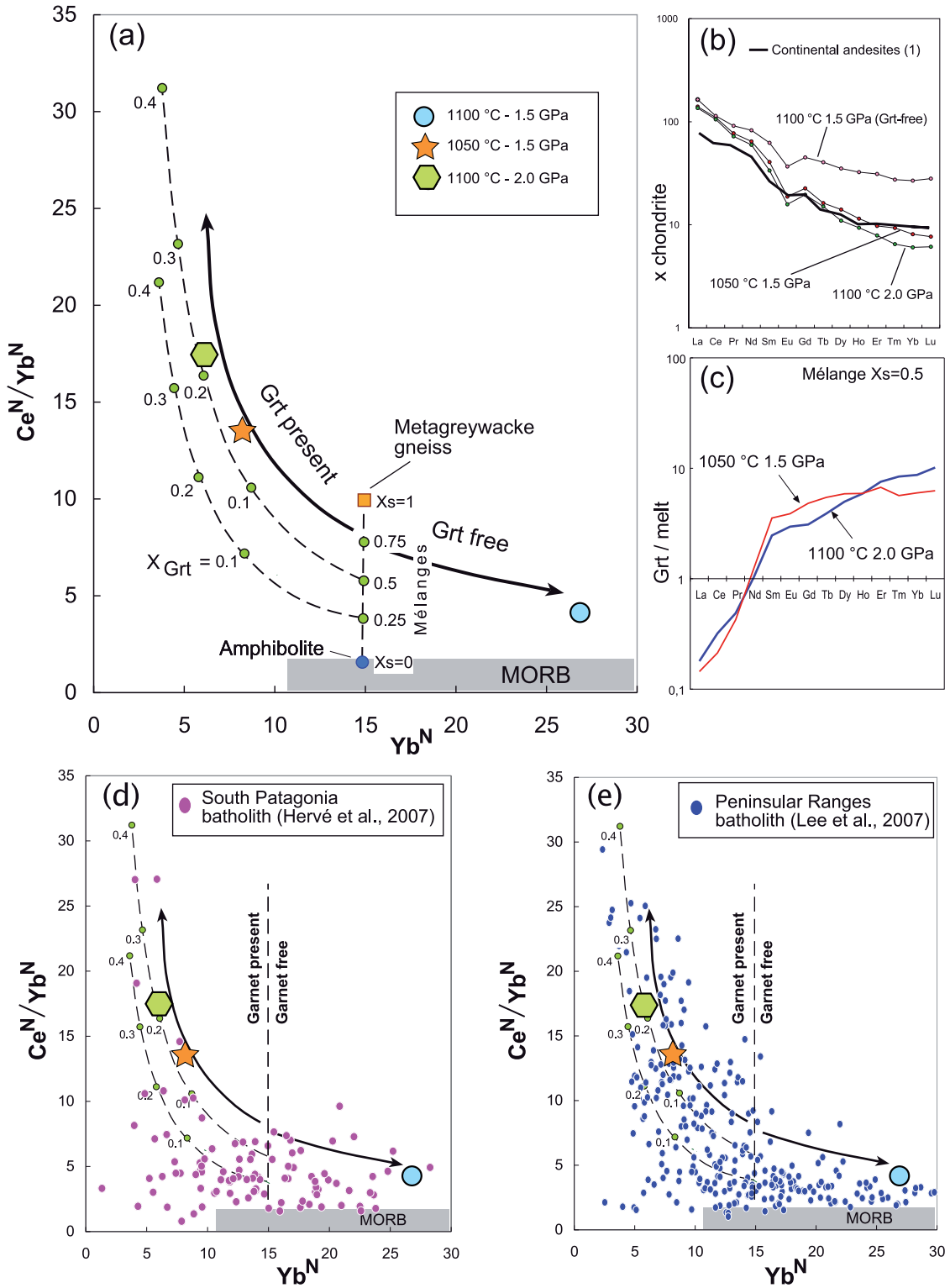

Fig. 10. REE patterns of experimental melts in Grt-present and Grt-free assemblages. (a) Progressive depletion in HREE (dashed curves) in the melt as a function of the amount of Grt in the system, modelled with the Grt/liquid partitioning coefficients (K_d) obtained in our experiments. Chondrite-normalized REE patterns are illustrated in (b) and the Grt/melt K_d values in (c). Numbers on the evolution lines in (a) indicate the fraction of Grt left in the residue. The two model lines correspond to mélanges with a fraction of gneiss (X_s) of 0·25 and 0·5. Cordilleran batholiths from South America and the Peninsular Ranges (d, e) show variable Ce_N/Yb_N and Yb_N contents.

parallel to the theoretical trend of Grt fractionation. The fractionation effect will depend on the amount of Grt in the residue. A large abundance of Grt does not necessarily mean a higher pressure in the source. It may also be due to a lower temperature of melt generation. Melts developed within the range 1050–1100°C (*c.* 60 vol. % melting) in the mixed source have a granodiorite composition and can display significant HREE depletion as a result of the presence of residual Grt in the source. It should be noted that the abundance of Grt in the residue increases with decreasing T. Thus, the fractionating effect will be more pronounced in lower T melts developed at lower melting degrees from the same source. These predictions match the observed REE patterns of natural granitoids, which vary from less fractionated and less silicic to more fractionated and more silicic. In general terms, melts developed at higher T have a greater probability of being generated in a Grt-free environment compared with lower T melts.

The homogeneous composition of hybrid melts from a heterogeneous source

The homogeneous composition of the melts produced in the multilayer capsules, which preserved the original layered structure, indicates that the melts are homogenized by inter-diffusion. The end result is modal heterogeneity in a composite system that reached chemical equilibrium. Similar results were obtained by Johnston & Wyllie (1988) in experiments with basalt–granite composite capsules. Although the layered structure is preserved in the composite capsules, the composition of the melts is almost identical across the layers. Homogenization may be favoured across the interface between the contrasting layers by a combination of crystal dissolution and precipitation, coupled with volume diffusion as proposed for peridotite melting systems (Lo Cascio *et al.*, 2008). The whole system is finally in chemical equilibrium independently of the location of phases in specific bands. The consequence is that a composite source may produce a homogeneous hybrid melt in equilibrium with a complex layered residue. Only in the case where melts are extracted rapidly from the composite source are two different magmas produced (Skjerlie & Patiño Douce, 1995). The long residence times of mantle wedge plumes predicted by our numerical modelling (several tens of million years, Fig. 2), favour the equilibration of the melt compositions. Also, the sublithospheric location of the mantle wedge plumes implies that the melt is more likely to remain in the source for longer, a process differing considerably from that of partial melting in continental collision settings, where melt segregation is normally accompanied by tectonically induced deformation that favours fast melt segregation (Brown & Rushmer, 1997).

Thermomechanical modelling predicts dynamic mixing of the mélange components (basalts and sediments) by long-lived plastic flow during transport within the mantle. Subducted mélanges are probably mixed at a scale of metres before they reach melting conditions. The size of blocks and layers of contrasted composition in exposed subduction mélanges ranges from kilometre- to millimetre-scale (Phipps, 1984). However, block sizes exhibit negative power-law (fractal) distribution in many mélanges (Medley, 2002) and, although there is not a typical size, most blocks are smaller than 10–20 m. Coherent interspersed horizons are also commonly less than a few tens of metres in thickness (Bell, 1982; Lash, 1987). Simple estimation of melt homogenization by ionic diffusion across the interface of the contrasted layers and blocks in mélanges shows that the time available for partial melting inside mantle wedge plumes (up to 20–30 Myr) may be sufficient to homogenize melt compositions over distances approaching 100 m.

The effect of heterogeneous layers and variable proportions of end-members

An important result from this study is the relatively uniform composition of the granodiorite melts obtained from the composite capsules with variable proportions of sedimentary and basaltic components. It was noted earlier that this is due to the buffering effect of the coexisting mineral assemblage Grt + Cpx + Pl + Melt, which is stable in the broad range of the studied bulk compositions and P–T conditions. This result is important in understanding the geochemical characteristics of granodiorite batholiths: they display very homogeneous major element compositions (Kemp *et al.*, 2003) but substantial variation in radiogenic isotopic composition, suggesting widely varying proportions of mantle and crustal components in their source. Our results provide a satisfactory explanation for both.

The buffering capability of the experimentally determined four-phase assemblage Grt + Cpx + Pl + Melt can be clearly seen in the isothermal–isobaric AKCF diagram of Fig. 6. Despite the large compositional variations between the different bulk-rock compositions ($X_s = 0{\cdot}75$–$0{\cdot}25$) used in the experiments, it can be readily appreciated that the compositions of the experimental melts are very similar. Except for the three-phase assemblage Grt + Cpx + Melt, developed during melting of the end-member MORB amphibolite sample and Grt + Pl + Melt during melting of the end-member sediment, all the other experiments have four phases (Grt + Cpx + Pl + Melt; bulk-rock compositions $X_s = 0{\cdot}75$ and $0{\cdot}25$). At constant P–T conditions, as the bulk-rock composition changes from that of MORB amphibolite, clinopyroxene is lost, the grossular content of the garnet decreases and the melt composition changes from

metaluminous to peraluminous. These changes in composition are, however, subtle for the lower-variance assemblage Grt + Cpx + Pl + Melt, confirming the buffering capability of the assemblage. This result is clearly illustrated by the almost identical composition of the melts from contrasted bulk-rock compositions in the range $X_s = 0{\cdot}75$–$0{\cdot}25$ (Fig. 5).

In conclusion, our experimental results suggest that the composition of melts formed by partial melting of the end-member bulk compositions (Bt-gneiss and amphibolite) is not buffered below 1100°C, 2 GPa, forming granitic (melting of gneiss) and tonalitic (melting of amphibolite) melts in high-variance assemblages Melt + Grt + Pl and Melt + Grt + Cpx, respectively. However, the composition of melts formed by partial melting of gneiss–amphibolite mélanges is 'buffered' in the intermediate compositional range ($X_s = 0{\cdot}25$–$0{\cdot}75$), forming granodioritic melts in the lower-variance phase assemblage Melt + Grt + Cpx + Pl. The implication is that granodiorites and tonalites represent cotectic melts that change to more mafic composition with increasing T and melt fraction.

Geological implications: towards a new scenario for arc magmatism

Cordilleran-type andesites and batholiths are closely associated in space and time in active continental margins and both are clearly related to subduction. Although the petrogenesis of andesitic magmas is a hotly debated topic, it is an observational fact that bulk mixtures of basalt plus sediment can replicate the composition of andesites and that, consequently, a high melt fraction derived from this source may also have an andesitic composition. Melt fractions of the order of 50 vol. % from a basalt–sediment mélange at a temperature of 1050–1100°C will produce melts of granodiorite to tonalite composition. According to the results of our numerical modelling, underplated plumes of partially molten mélange material could be emplaced at the base of the lithospheric mantle, more than 200 km away from the trench, where they could reside for millions of years. Figure 11 shows a detailed section of the underplated plume model used here to constrain the experimental conditions. At the interface of the mélange with the surrounding mantle reaction with peridotite results in a Px-rich aureole that prevents further reaction, making it possible for the silicic plume to survive in the mantle for a long time (Castro & Gerya, 2008). There is a continuous variation from top to bottom in the plume, in melt fraction and melt composition. Extraction of melts from the plume head to form a batholith within the crust needs a tectonic change from compressional to extensional. Such a switch from compressional to extensional tectonics in the overriding plate is commonly observed in the geological record (Collins, 2002), and is related to changes in a number of key parameters affecting the kinematics, dynamics and rheology of the converging plates (age of the subducting slab, subduction of oceanic plateaux, fluid pressure in the sediments, rate of convergence, and weakness of the overriding lithosphere, among others). The cyclicity of magmatic and tectonic episodes in the North American Cordilleran batholiths (DeCelles *et al.*, 2009) is consistent with the plume model. Plume generation at the Benioff plane is repeated periodically with alternating mixed (mantle and crust materials) and unmixed (only partially molten peridotite) plumes on a timescale of millions to tens of million years (Gerya & Yuen, 2003*b*; Gerya *et al.*, 2006). Ultrahigh-resolution numerical experiments (Gerya *et al.*, 2004; Gorczyk *et al.*, 2007*a*) show that the growth of a single large plume can also be cyclic on a timescale of around 1 Myr, which can potentially cause magmatic pulses within a batholith formed from the plume.

According to this silicic plume model for arc magmatism, a large part of the new material added to continental margins is derived from subducted oceanic crust and sediments, with limited involvement of peridotite-derived melts similar to those dominating crustal addition in oceanic island arcs (e.g. Nikolaeva *et al.*, 2008). The latter are predominantly basaltic andesites and andesites, and their equivalent plutonic rocks (diorites and gabbros). Our new model implies a global process of partial melting of subducted oceanic crust plus its sedimentary cover at active continental margins, adding a net flux of diorite to granodiorite composition to the continents. This melt flux from silicic, mantle wedge plumes matches the overall composition of the continental crust and strongly supports the 'andesite model' for the origin of the continents (Weaver & Tarney, 1982); it minimizes the need for removal of a mafic component from the continental crust required by models that assume a basaltic net flux from the mantle in active margins. The refractory residue left behind by the granodiorite–tonalite melts after extraction from the plume can remain in the upper mantle or become emplaced within the lower continental crust forming mafic granulite complexes. Another significant form of crustal addition, predicted by the numerical models (e.g. Gorczyk *et al.*, 2007*a*; Nikolaeva *et al.*, 2008; Sizova *et al.*, 2009), consists of magmatic rocks produced by partial melting of hydrated mantle formed atop the subducting slab.

CONCLUSIONS

Our experimental results suggest that the composition of melts formed by partial melting of a single end-member (either greywacke or MORB) is not buffered, forming either granitic (melting of greywacke) or tonalitic (melting of MORB) liquids. In contrast, the compositions of melts formed after by partial melting of greywacke–MORB mélanges are buffered by Grt + Cpx + Pl in the residue. These cotectic melts are geochemically (major and trace elements) comparable with those of volcanic and plutonic

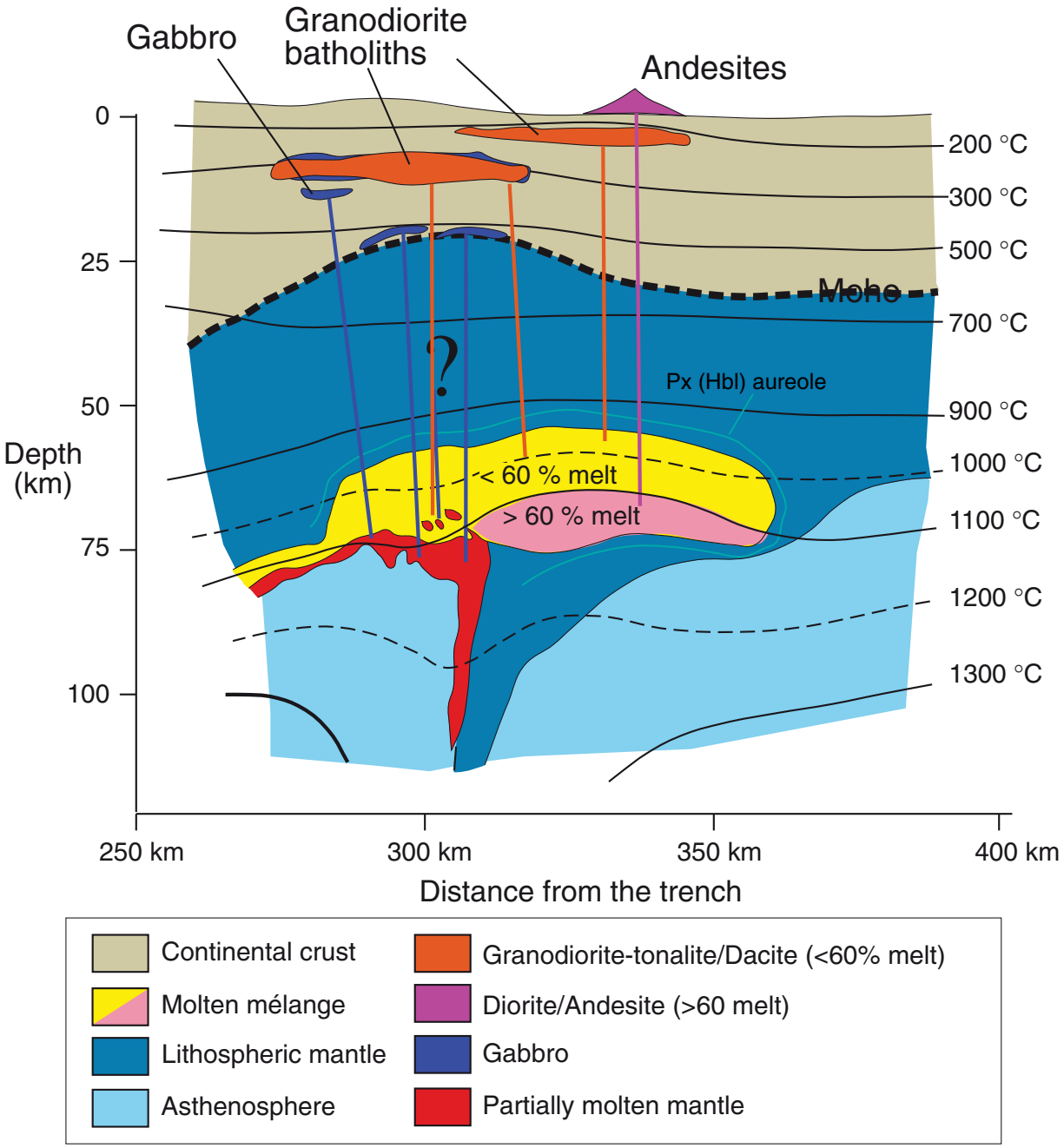

Fig. 11. Model scenario for the generation of granodiorite–tonalite batholiths by variable degree of partial melting of an underplated cold mantle wedge plume emplaced near the bottom of the upper plate lithosphere (enlarged area from Fig. 2). The 1100°C isotherm separates two zones within the plume. Granodiorite and tonalite melt compositions may be developed within the upper zone of the plume at melt fractions of about 60 vol. %. The model also predicts a partially molten region in the peridotite mantle that produces subordinate mafic melts that are infrequently associated with granodiorite–tonalite batholiths in continental margin arcs.

rocks within magmatic arcs associated with subduction at active continental margins. According to this model, the growth of the continental crust at convergent continental margins may take place by a net flux of primary silicic magmas with bulk tonalitic to granodioritic composition, generated by sub-lithospheric melting of tectonic mélanges composed of a mixture of subducted oceanic crust and sediment. Such mélanges are emplaced as underplated cold 'plumes' at the base of the upper plate continental lithosphere.

ACKNOWLEDGEMENTS

We thank Jim Beard, Wolfgang Siebel and an anonymous reviewer for constructive criticism. Comments and criticism by editor Ron Frost contributed to improving the original manuscript and to presenting our model in a more robust way.

FUNDING

We acknowledge with thanks financial support from the Spanish Ministry of Science and Innovation (Project CGL2007-63237/BTE). The manuscript was completed during the sabbatical leave of the first author (A.C.) at ETH-Zurich in 2009 (Grant PR2008-0280). This work was supported by ETH Research Grants TH-12/05-3, TH-0807-3, SNF Research Grant 200021-113672/1, 200021-116381/1 and the RF President Program 'Leading Scientific School of Russia' (Grant 1949.2008.5) to T.V.G.

REFERENCES

Allègre, C. J. & Ben Othman, D. (1980). Nd–Sr isotopic relationship in granitoid rocks and continental crust development: a chemical approach to orogenesis. *Nature* **286**, 335–341.

Annen, C. & Sparks, R. S. J. (2002). Effects of repetitive emplacement of basaltic intrusions on thermal evolution and melt generation in the crust. *Earth and Planetary Science Letters* **203**, 937–955.

Annen, C., Blundy, J. D. & Sparks, R. S. J. (2006). The genesis of intermediate and silicic magmas in deep crustal hot zones. *Journal of Petrology* **47**, 505–539.

Barton, M. D., Staude, J. M., Snow, E. A. & Johnson, D. A. (1991). Aureole systematics. In: Kerrick, D. M. (ed.) *Contact Metamorphism. Mineralogical Society of America, Reviews in Mineralogy* **26**, 723–847.

Bea, F., Fershtater, G. B., Montero, P., Smirnov, V. N. & Molina, J. F. (2005). Deformation-driven differentiation of granitic magma: the Stepninsk pluton of the Uralides, Russia. *Lithos* **81**, 209–233.

Beard, J. S., Ragland, P. C. & Crawford, M. L. (2005). Reactive bulk assimilation: A model for crust–mantle mixing in silicic magmas. *Geology* **33**, 681–684.

Bell, C. M. (1982). The Lower Paleozoic metasedimentary basement of the Coastal Ranges of Chile between 25°30′ and 27°S. *Revista Geológica de Chile* **17**, 21–29.

Blundy, J. D. & Sparks, R. S. J. (1992). Petrogenesis of mafic inclusions in granitoids of the Adamello Massif, Italy. *Journal of Petrology* **33**, 1039–1104.

Brown, M. & Rushmer, T. (1997). The role of deformation in the movement of granite melt: views from laboratory and the field. In: Holmes, M. B. (ed.) Deformation-*Enhanced* Fluid Transport in the Earth's Crust and Mantle. London: Chapman & Hall, pp. 111–144.

Castro, A. & Gerya, T. V. (2008). Magmatic implications of mantle wedge plumes: Experimental study. *Lithos* **103**, 138–148.

Castro, A. & Stephens, W. E. (1992). Amphibole-rich polycrystalline clots in calc-alkaline granitic rocks and related enclaves. *Canadian Mineralogist* **30**, 1093–1112.

Castro, A., Patiño Douce, A. E., Corretgé, L. G., De La Rosa, J. D., El-Biad, M. & El-Hmidi, H. (1999). Origin of peraluminous granites and granodiorites, Iberian massif, Spain. *An experimental test of granite petrogenesis.* Contributions to Mineralogy and Petrology **135**, 255–276.

Castro, A., Corretgé, L. G., El-Biad, M., El-Hmidi, H., Fernández, C. & Patiño Douce, A. (2000). Experimental constraints on Hercynian anatexis in the Iberian Massif, Spain. *Journal of Petrology* **41**, 1471–1488.

Castro, A., Corretgé, L. G., De La Rosa, J. D., Fernández, C., López, S. & Chacón, H. (2003). The appinite–migmatite complex of Sanabria, NW Iberian Massif, Spain. *Journal of Petrology* **44**, 1309–1334.

Castro, A., Garcia-Casco, A., Fernández, C., Corretgé, L. G., Moreno-Ventas, I., Gerya, T. & Low, I. (2009). Ordovician ferrosilicic magmas: Experimental evidence for ultrahigh temperatures affecting a metagreywacke source. *Gondwana Research* **16**, 622–632.

Cobbing, E. J., Pitcher, W. S., Wilson, J. J., Baldock, J. W., Taylor, W. P., McCourt, W. & Snelling, N. J. (1981). *The Geology of the Western Cordillera of Northern Peru.* London: Institute of Geological Sciences, Natural Environment Research Council.

Collins, W. J. (2002). Hot orogens, tectonic switching, and creation of continental crust. *Geology* **30**, 535–538.

Condie, K. C. (1997). *Plate Tectonics and Crustal Evolution.* Oxford: Butterworth–Heinemann.

Costa, F., Scaillet, B. & Pichavant, M. (2004). Petrological and experimental constraints on the pre-eruption conditions of Holocene dacite from Volcán San Pedro (36°S, Chilean Andes) and the importance of sulphur in silicic subduction-related magmas. *Journal of Petrology* **45**, 855–881.

Currie, C. A., Beaumont, C. & Huismans, R. (2007). The fate of subducted sediments: A case for backarc intrusion and underplating. *Geology* **35**, 1111–1114.

DeCelles, P. G., Ducea, M. N., Kapp, P. & Zandt, G. (2009). Cyclicity in Cordilleran orogenic systems. *Nature Geoscience* **2**, 251–257.

De Paolo, D. J. (1981). A neodymium and strontium isotopic study of the Mesozoic calc-alkaline granitic batholiths of the Sierra Nevada and Peninsular Ranges, California. *Journal of Geophysical Research* **86**, 10470–10488.

Ducea, M. (2001). The California arc: Thick granitic batholiths, eclogitic residues, lithospheric-scale thrusting, and magmatic flare-ups. *GSA Today* **11**, 4–10.

Fernández, C., Becchio, R., Castro, A., Viramonte, J. M., Moreno-Ventas, I. & Corretge, L. G. (2008). Massive generation of atypical ferrosilicic magmas along the Gondwana active margin: Implications for cold plumes and back-arc magma generation. *Gondwana Research* **14**, 451–473.

Fowler, M. B., Henney, P. J., Darbyshire, D. P. F. & Greenwood, P. B. (2001). Petrogenesis of high Ba–Sr granites: The Rogart pluton, Sutherland. *Journal of the Geological Society, London* **158**, 521–534.

Frost, C. D., Bell, J. M., Frost, B. R. & Chamberlain, K. R. (2001). Crustal growth by magmatic underplating: Isotopic evidence from the Northern Sherman batholith. *Geology* **29**, 515–518.

Gerya, T. V. & Stoeckhert, B. (2006). 2-D numerical modeling of tectonic and metamorphic histories at active continental margins. *International Journal of Earth Sciences* **95**, 250–274.

Gerya, T. V. & Yuen, D. A. (2003*a*). Characteristics-based marker-in-cell method with conservative finite-differences schemes for modeling geological flows with strongly variable transport properties. *Physics of the Earth and Planetary Interiors* **140**, 293–318.

Gerya, T. V. & Yuen, D. A. (2003*b*). Rayleigh–Taylor instabilities from hydration and melting propel 'cold plumes' at subduction zones. *Earth and Planetary Science Letters* **212**, 47–62.

Gerya, T. V., Yuen, D. A. & Sevre, E. O. D. (2004). Dynamical causes for incipient magma chambers above slabs. *Geology* **32**, 89–92.

Gerya, T. V., Connolly, J. A. D., Yuen, D. A., Gorczyk, W. & Capel, A. M. (2006). Seismic implications of mantle wedge plumes. *Physics of the Earth and Planetary Interiors* **156**, 59–74.

Gerya, T.V., Perchuk, L. L. & Burg, J.-P. (2008). Transient hot channels: perpetrating and regurgitating ultrahigh-pressure, high-temperature crust–mantle associations in collision belts. *Lithos* **103**, 236–256.

Gerya, T. V., Fossati, D., Cantieni, C. & Seward, D. (2009). Dynamic effects of aseismic ridge subduction: numerical modelling. *European Journal of Mineralogy* **21**, 649–661.

Gorczyk, W., Gerya, T. V., Connolly, J. A. D. & Yuen, D. A. (2007*a*). Growth and mixing dynamics of mantle wedge plumes. *Geology* **35**, 587–590.

Gorczyk, W., Guillot, S., Gerya, T.V. & Hattori, K. (2007*b*). Asthenospheric upwelling, oceanic slab retreat and exhumation of UHP mantle rocks: insights from Greater Antilles. *Geophysical Research Letters* doi:10.1029/2007GL031059.

Gorczyk, W., Willner, A. P., Gerya, T. V., Connolly, J. A. D. & Burg, J.-P. (2007*c*). Physical controls of magmatic productivity at Pacific-type convergent margins: New insights from numerical modeling. *Physics of the Earth and Planetary Interiors* **163**, 209–232.

Green, T. H. (1982). Anatexis of mafic crust and high pressure crystallization of andesite. In: Thorpe, R. S. (ed.) *Andesites: Orogenic Andesites and Related Rocks*. Chichester: John Wiley, pp. 465–487.

Grove, T. L., Baker, M. B., Price, R. C., Parman, S. W., Elkins-Tanton, L. T., Chatterjee, N. & Muntener, O. (2005). Magnesian andesite and dacite lavas from Mt. Shasta, northern California: Products of fractional crystallization of H2O-rich mantle melts. *Contributions to Mineralogy and Petrology* **148**, 542–565.

Hall, L. J., Brodie, J., Wood, B. J. & Carroll, M. R. (2004). Iron and water losses from hydrous basalts contained in $Au_{80}Pd_{20}$ capsules at high pressure and temperature. *Mienralogical Magazine* **68**, 75–81.

Hawkesworth, C. J. & Kemp, A. I. S. (2006). Evolution of the continental crust. *Nature* **443**, 811–817.

Hervé, F., Pankhurst, R. J., Fanning, C. M., Calderon, M. & Yaxley, G. M. (2007). The South Patagonian batholith: 150 my of granite magmatism on a plate margin. *Lithos* **97**, 373–394.

Hildreth, W. & Moorbath, S. (1988). Crustal contributions to arc magmatism in the Andes of Central Chile. *Contributions to Mineralogy Petrology* **98**, 455–489.

Johnston, A. D. & Wyllie, P. J. (1988). Interaction of granitic and basic magmas: experimental observations on contamination processes at 10 kbar with H_2O. *Contributions to Mineralogy and Petrology* **98**, 352–362.

Kelemen, P. B. (1995). Genesis of high-Mg andesites and the continental crust. *Contributions to Mineralogy and Petrology* **120**, 1–19.

Kelemen, P. B., Hanghoj, K. & Greene, A. R. (2003). One view of the geochemistry of subduction-related magmatic arcs, with emphasis on primitive andesite and lower crust. In: Rudnick, R. L. (ed.) *The Crust*. Amsterdam: Elsevier, pp. 593–659.

Kemp, A. I. S., Hawkesworth, C. J., Heinrich, D. H. & Karl, K. T. (2003). Granitic perspectives on the generation and secular evolution of the continental crust. In: Rudnick, R. L. (ed.) The Crust. Amsterdam: Elsevier, pp. 349–410.

Kretz, R. (1983). Symbols for rock-forming minerals. *Am Mineral* **68**, 277–279.

Lash, G. G. (1987). Diverse mélanges of an ancient subduction complex. *Geology* **15**, 652–655.

Lee, C.-T. A., Morton, D. M., Kistler, R. W. & Baird, A. K. (2007). Petrology and tectonics of Phanerozoic continent formation: From island arcs to accretion and continental arc magmatism. *Earth and Planetary Science Letters* **263**, 370–387.

Lo Cascio, M., Liang, Y., Shimizu, N. & Hess, P. C. (2008). An experimental study of the grain-scale processes of peridotite melting: Implications for major and trace element distribution during equilibrium and disequilibrium melting. *Contributions to Mineralogy and Petrology* **156**, 87–102.

López, S. & Castro, A. (2001). Determination of the fluid-absent solidus curve and supersolidus phase relationships of MORB-derived amphibolites in the range 4–14 kbar. *American Mineralogist* **86**, 1396–1403.

Maaloe, S. & Wyllie, P. J. (1975). Water content of a granite magma deduced from the sequence of crystallization determined experimentally with water-undersaturated conditions. *Contributions to Mineralogy and Petrology* **52**, 175–191.

Massey, N. W. D., Mcintyre, D. G., Desjardins, P. J. & Cooney, R. T. (2005). *Geology of British Columbia. Geoscience Map 2005–3, Scale 1:1 000 000*. Vancouver: British Columbia Geological Survey.

McCulloch, M. T. & Gamble, J. A. (1991). Geochemical and geodynamical constraints on subduction zone magmatism. *Earth and Planetary Science Letters* **102**, 358–374.

Medley, E. W. (2002). Estimating block size distributions of mélanges and similar block-in-matrix rocks (Bimrocks). In: Hammah, R., Bawden, W., Curran, J. & Telesnicki, M. (eds) *Proceedings of the 5th North American Rocks Mechanics Symposium*. Toronto, Ont: University of Toronto Press, pp. 599–606.

Moore, G. & Carmichael, I. S. E. (1998). The hydrous phase equilibria (to 3 kbar) of an andesite and basaltic andesite from western Mexico: constraints on water content and conditions of phenocryst growth. *Contributions to Mineralogy and Petrology* **130**, 304–319.

Naney, M. T. (1983). Phase equilibria of rock-forming ferromagnesian silicates in ganitic systems. *American Journal of Science* **283**, 993–1033.

Nikolaeva, K., Gerya, T. V. & Connolly, J. A. D. (2008). Numerical modelling of crustal growth in intraoceanic volcanic arcs. *Physics of the Earth and Planetary Interiors* **171**, 336–356.

Pankhurst, R. J., Weaver, S. D., Herve, F. & Larrondo, P. (1999). Mesozoic–Cenozoic evolution of the North Patagonian Batholith in Aysen, southern Chile. *Journal of the Geological Society, London* **156**, 673–694.

Parada, M. A., Nyström, J. O. & Levi, B. (1999). Multiple sources for the Coastal Batholith of central Chile 31–34°S: geochemical and Sr–Nd isotopic evidence and tectonic implications. *Lithos* **46**, 504–521.

Patiño-Douce, A. E. (1995). Experimental generation of hybrid silicic melts by reaction of high-Al basalt with metamorphic rocks. *Journal of Geophysical Research* **100**, 15623–15639.

Patiño Douce, A. E. (1999). What do experiments tell us about the relative contributions of crust and mantle to the origin of granitic magmas? In: Castro, A., Fernández, C. & Vigneresse, J. L. (eds) *Understanding Granites. Integrating New and Classical Techniques. Geological Society, London, Special Publications* **158**, 55–75.

Petford, N. & Gallagher, K. (2001). Partial melting of mafic (amphibolitic) lower crust by periodic influx of basaltic magma. *Earth and Planetary Science Letters* **193**, 483–489.

Phipps, S. P. (1984). Ophiolitic olistostromes in the basal Great Valley sequence, Napa County, Northern California Coast Ranges. In: Raymond, L. A. (ed.) *Mélanges: Their Nature, Origin and Significance. Geological Society of America, Special Papers* **198**, 103–125.

Pichavant, M., Mysen, B. O. & Macdonald, R. (2002). Source and H_2O content of high-MgO magmas in island arc settings: an experimental study of a primitive calc-alkaline basalt from St. Vincent, Lesser Antilles arc. *Geochimica et Cosmochimica Acta* **66**, 2193–2209.

Presnall, D. C. & Bateman, P. C. (1973). Fusion relations in the system $NaAlSi_3O_8$–$CaAl_2Si_2O_8$–$KAlSi_3O_8$–SiO_2–H_2O and generation of granitic magmas in the Sierra Nevada batholith. *Geological Society of America Bulletin* **84**, 3181–3201.

Scaillet, B. & Pichavant, M. (2003). Experimental constraints on volatile abundances in arc magmas and their implications for degassing processes. In: Oppenheimer, C., Pyle, D. M. & Barclay, J. (eds) *Volcanic degassing*. Geological Society, London, Special Publications **213**, pp. 23–52.

Shreve, R. L. & Cloos, M. (1986). Dynamics of sediment subduction, mélange formation, and prism accretion. *Journal of Geophysical Research* **91**, 10229–10245.

Sizova, E., Gerya, T., Brown, M. & Perchuk, L. L. (2009). Subduction styles in the Precambrian: Insight from numerical experiments. *Lithos*, doi:10.1016/j.lithos.2009.05.028.

Skjerlie, K. P. & Patiño Douce, A. E. (1995). Anatexis of interlayered amphibolite and pelite at 10 kbar: Effect of diffusion of major components on phase relations and melt fraction. *Contributions to Mineralogy and Petrology* **122**, 62–78.

Stern, C. R. (1991). Role of subduction erosion in the generation of Andean magmas. *Geology* **19**, 78–81.

Taylor, S. R. & McLennan, S. M. (1985). *The Continental Crust: Its Composition and Evolution*. Melbourne: Blackwell.

Thompson, A. B., Matile, L. & Ulmer, P. (2002). Some thermal constraints on crustal assimilation during fractionation of hydrous, mantle-derived magmas with examples from Central Alpine Batholiths. *Journal of Petrology* **43**, 403–422.

Ugidos, J. M. & Recio, C. (1993). Origin of cordierite-bearing granites by assimilation in the Central Iberian Massif (CIM), Spain. *Chemical Geology* **103**, 27–43.

Van Huenen, J., van den Berg, A.P. & Vlaar, N.J. (2000). A thermo-mechanical model of horizontal subduction below an overriding plate. *Earth and Planetary Science Letters* **182**, 157–169.

Von Huene, R. & Scholl, D. W. (1991). Observations at convergent margins concerning sediment subduction, subduction erosion. *Reviews of Geophysics* **29**, 279–316.

Weaver, B. L. & Tarney, J. (1982). Andesitic magmatism and continental growth. In: Thorpe, R. S. (ed.) *Andesites: Orogenic Andesites and Related Rocks*. Chichester: John Wiley, pp. 639–661.

Wyllie, P. J. (1977). From crucibles through subduction to batholiths. In: Saxena, S. K. & Bhattacharjia, S. (eds) *Energetics of Geological Processes*. Berlin: Springer, pp. 389–433.